Am J Physiol Renal Physiol 299: F1094–F1110, 2010.
First published August 18, 2010; doi:10.1152/ajprenal.00056.2010.

Fibroblast growth factor-10 signals development of von Brunn's nests in the exstrophic bladder

Rocky Eastman Jr.,[1] Elizabeth M. Leaf,[1] Dianzhong Zhang,[1] Lawrence D. True,[2] Robert M. Sweet,[4] Kristy Seidel,[5] Joseph R. Siebert,[2,3,6] Richard Grady,[4,7] Michael E. Mitchell,[4,7] and James A. Bassuk[1,4,7]

[1]*Program in Human Urothelial Biology, Center for Tissue and Cell Sciences, and* [5]*Office of Biostatistical Services, Seattle Children's Research Institute; Departments of* [2]*Pathology,* [3]*Pediatrics, and* [4]*Urology, University of Washington School of Medicine; and* [6]*Department of Laboratories and* [7]*Division of Pediatric Urology, Seattle Children's Hospital, Seattle, Washington*

Submitted 29 January 2010; accepted in final form 16 August 2010

Eastman R, Leaf EM, Zhang D, True LD, Sweet RM, Seidel K, Siebert JR, Grady R, Mitchell ME, Bassuk JA. Fibroblast growth factor-10 signals development of von Brunn's nests in the exstrophic bladder. *Am J Physiol Renal Physiol* 299: F1094–F1110, 2010. First published August 18, 2010; doi:10.1152/ajprenal.00056.2010.—von Brunn's nests have long been recognized as precursors of benign lesions of the urinary bladder mucosa. We report here that von Brunn's nests are especially prevalent in the exstrophic bladder, a birth defect that predisposes the patient to formation of bladder cancer. Cells of von Brunn's nest were found to coalesce into a stratified, polarized epithelium which surrounds itself with a capsule-like structure rich in types I, III, and IV collagen. Histocytochemical analysis and keratin profiling demonstrated that nested cells exhibited a phenotype similar, but not identical, to that of urothelial cells of transitional epithelium. Immunostaining and in situ hybridization analysis of exstrophic tissue demonstrated that the FGF-10 receptor is synthesized and retained by cells of von Brunn's nest. In contrast, FGF-10 is synthesized and secreted by mesenchymal fibroblasts via a paracrine pathway that targets basal epithelial cells of von Brunn's nests. Small clusters of 10pRp cells, positive for both FGF-10 and its receptor, were observed both proximal to and inside blood vessels in the lamina propria. The collective evidence points to a mechanism where von Brunn's nests develop under the control of the FGF-10 signal transduction system and suggests that 10pRp cells may be the original source of nested cells.

bladder; epithelium; exstrophy; growth factors; urothelium; lamina propria

VON BRUNN'S NESTS ARE GROUPS of proliferating epithelial cells commonly found in the adult lower urinary tract. These proliferative lesions are prevalent in the adult bladder, with autopsy studies showing that 89% of grossly normal bladders exhibit this histological condition (55). The frequency of von Brunn's nest in normal pediatric bladders is undocumented, presumably due to the lack of sufficient sampling.

An increased risk of cancer in the exstrophic bladder has been known for over 50 years (5). At a mean age of 40 yr, the risk of bladder cancer has been reported to be 694 times that of the normal population (56), equating to an incidence of 3,884 cases per 100,000 (43). The role of environmental injury in carcinogenesis is widely recognized. Malignancy in exstrophic bladders has been reported most frequently in untreated adults and those undergoing surgical treatments which involve the mixing of fecal and urinary systems during enterocystoplastic augmentation (37). Less known is the role that proliferative lesions such as von Brunn's nests may play in carcinoma development, with some reports regarding nests as precancerous (34) while other literature contests this notion (37, 40, 55).

When the epithelial cells lining the central lumen of von Brunn's nests undergo cystic degenerative changes, cystitis cystica develops. Metaplasia of the nest epithelium to a columnar type results in cystitis glandularis. Cystitis cystica and cystitis glandularis also have high incidence rates in normal adult bladders, reported at 60 (55) and 28% (40), respectively. Cystitis glandularis is considered a premalignant disease of the lower urinary tract by some researchers, with several reports suggesting it is a precursor to adenocarcinoma (15, 28, 35, 37). Other reports refute this (11, 14, 55). There are also recent data supporting the premalignant potential of the intestinal type of cystitis glandularis (6) and refuting it (10). Such uncertainty has led to a diagnostic dilemma and the misdiagnosis of cystitis glandularis as a cancer clinically and radiologically (42).

The majority of the literature on von Brunn's nests and cystitis glandularis consists of case reports and studies of the clinical progression of this entity. A better understanding of cellular development and differentiation of von Brunn's nests is therefore essential to the diagnosis and treatment of this histopathological condition and to determine its role in carcinogenesis. The role of growth factors in von Brunn's nest-dependent processes is unknown.

FGFs interact with their cell-surface tyrosine kinase receptors (FGFRs) to mediate, among other cellular processes, cell proliferation, differentiation, and migration, as well as to stimulate tissue repair. The best-studied FGF in the urinary bladder is FGF-10, a 22-kDa polypeptide which is expressed in lamina propria and transported to the urothelium, where it interacts with its cell surface receptor to stimulate urothelial cell proliferation (2, 58). The FGF-10 pathway is the principal compensatory paracrine mechanism that defines the urothelial response to injury in partial bladder outlet obstruction (27). Because recombinant FGF-10 therapy is able to rescue a deficient urothelium found in mice that harbor a targeted disruption of the *FGF-7* gene (2), the growth factor is considered to have significant clinical potential.

The cell-surface FGF-10 receptor is composed of an extracellular domain containing two or three immunoglobulin-like loops, a transmembrane segment, and an intracellular split tyrosine kinase domain. The C terminus of immunoglobulin loop III determines ligand specificity for FGFRs. Loop III undergoes alternative mRNA splicing to yield three different

Address for reprint requests and other correspondence: J. A. Bassuk, Program in Human Urothelial Biology, Center for Tissue and Cell Sciences, Seattle Children's Research Institute, 1900 9th Ave., Mailstop C9S-5, Seattle, WA 98101 (e-mail: james.bassuk@seattlechildrens.org).

 0363-6127/10 Copyright © 2010 the American Physiological Society

RIGHTSLINK www.physiology.org/journal/ajprenal by ${individualUser.givenNames} ${individualUser.surname} (037.055.225.009) on June 10, 2018.
Copyright © 2010 American Physiological Society. All rights reserved.

splice variants: IIIa, IIIb, and IIIc. Variant IIIa codes for a secreted FGF-binding protein, while variants IIIb and IIIc encode membrane-bound receptors. It has been shown that FGF-10 stimulates urothelial cell proliferation via the FGF-10 receptor, which is encoded by the IIIb mRNA splice variant to stimulate urothelial cell proliferation (2, 58). While the IIIb mRNA splice variant of the *FGFR2* gene is expressed in many types of epithelial tissue, including transitional epithelium (2, 58), the IIIc variant is restricted to the mesenchyme. An isoform of FGF-10 has been detected within urothelial cell nuclei (25). The growth factor is able to cross the nuclear membrane via a nuclear localization signal (NLS), where it accumulates in the nucleus at high levels (25). Mutagenesis of this NLS abrogates the growth factor's mitogenic activity, suggesting that the function of nuclear FGF-10 may be to selectively maintain progression through the cell cycle and/or influence urothelial cell differentiation.

We report here that the FGF-10 pathway appears to be functional in bladder exstrophy and signals the development of von Brunn's nests. We also report on and discuss the origin of Brunn's nests in the human urinary bladder.

MATERIALS AND METHODS

Human Tissue

Human bladder mucosal tissue, composed of stratified epithelia adhered to its underlying lamina propria, was obtained as surgical explants with informed consent and/or assent under approval of the Institutional Review Board of Seattle Children's Hospital. The criterion of inclusion for the seven subjects included in this study was a diagnosis of bladder exstrophy. Foreskin was obtained from discarded surgical tissue. Explants were typically divided into equal portions for histology, cell culture, and RNA isolation.

Processing of Human Tissue for Histological Analysis

Surgically removed bladder tissue was fixed overnight in either FAA (4% vol/vol paraformaldehyde, 50% vol/vol ethanol, and 5% vol/vol acetic acid) or methyl Carnoys (60% vol/vol methanol, 30% vol/vol chloroform, and 10% vol/vol acetic acid). After washing, the fixed tissue was dehydrated through a series of graded ethanol concentrations followed by three 10-min incubations in xylene substitute (Sigma, St. Louis, MO). For all experiments in this study, specimens were embedded in paraffin, cut into 5- to 6-μm-thick sections, and mounted on Superfrost Plus microscope slides (Erie Scientific, Portsmouth, NH). Additionally, sections for mRNA detection with single-strand RNA probes were spread using diethylpyrocarbonate-treated water.

Masson's Trichrome Staining

Specimens were dewaxed, rehydrated, mordanted in Bouin's solution (Sigma) at 50°C for 1 h, and washed with water until the yellow color disappeared. Nuclei were stained with working Weigert's iron hematoxylin. After washing, sections were stained with a Masson's trichrome staining kit (catalog no. HT-15, Sigma) according to the manufacturer's instructions.

Nomenclature of Cytokeratins

Several nomenclatures for keratins, of which cytokeratins comprise an intracellular subset, have been proposed. A common nomenclature for cytokeratins is to preface the keratin number to the CK abbreviation (e.g., CK7, CK13, CK14, and CK17). The naming system of Moll et al. (32) has also been widely used (e.g., K7, K13, K14, and K17). The Human Genome Organization (HUGO) attempts to ensure that for each gene there is one name and one symbol. HUGO has thus implemented the KRT abbreviation to represent a specific keratin gene (e.g., *KRT7*, *KRT13, KRT14*, and *KRT17*). Because the overall present naming of keratins had not been systematic, a reorganized and durable scheme was proposed in 2006 (39). It is this latter nomenclature that is used in this report (e.g., *KRT7* for the gene and K7 for the protein).

Colorimetric Immunohistochemical Detection

Epitope detection was achieved with secondary antibodies conjugated to either alkaline phosphatase or horseradish peroxidase. Recognition of primary antibodies complexed to FGF-10 or the FGF-10 receptor was achieved with alkaline phosphatase, while antibodies complexed to collagen type IV, keratins (K) 7, 13, 14, and 17, and uroplakin III were detected with horseradish peroxidase. Controls omitting the primary antibody were run on parallel slides during all experiments.

Specimens detected with alkaline phosphatase were dewaxed and rehydrated, then incubated for 1 h with one of two blocking solutions. For FGF-10 detection, blocking was achieved with 5% normal rabbit serum in TBST [10 mM Tris·HCl (pH 7.5), 250 mM NaCl, and 0.3% (vol/vol) Tween 20]. For recognition of the FGF-10 receptor, blocking was completed with 1% (wt/vol) BSA (fraction V, Sigma) in TBST. Primary antibodies directed against human FGF-10 (catalog no. AF345) and the human FGF-10 receptor (catalog no. MAB665) were purchased from R&D Systems (Minneapolis, MN) as goat polyclonal and mouse monoclonal IgGs, respectively. The former was further affinity-purified using a previously described technique (3). After blocking, slides were incubated at room temperature for 4 h with either 1.67 μg/ml of the anti-FGF-10 IgG or 20 μg/ml of the receptor antibody, diluted in their respective blocking solutions. After a series of washes with TBST, sections were incubated at room temperature with secondary antibodies conjugated to alkaline phosphatase for 1 h. Secondary antibodies used were alkaline phosphatase-conjugated rabbit anti-goat IgG (3 μg/ml, catalog no. 305–055-045, Jackson ImmunoResearch, West Grove, PA) for FGF-10 detection and sheep anti-mouse IgG for detection of the FGF-10 receptor (1:100 dilution, catalog no. A3563, Sigma). Slides were then washed with TBST and rinsed with detection buffer at pH 9.5 (Roche Applied Science, Indianapolis, IN), followed by color development using substrates 4-nitro blue tetrazolium chloride and 5-bromo-4-chloro-3-indolyl-phosphate (Roche) in detection buffer. Images were acquired with a Leica DMR light microscope equipped with a Leica DC200 digital camera at image resolutions of 1,280 × 1,024 (6.7 μm/pixel).

For horseradish peroxidase-catalyzed reactions, dewaxed and rehydrated sections were subjected to heat-induced epitope retrieval by submersion in 1 liter of 10 mM citric acid (pH 6.0) and 10–16 min of microwaving. After cooling, sections were blocked for endogenous peroxidases by a 10-min incubation with 3% (vol/vol) hydrogen peroxide, washed with water, and assembled onto Sequenza coverplates (Thermo Scientific, Waltham, MA). After further blocking for endogenous avidin and biotin moities (DakoCytomation, Carpenteria, CA), a 1:10 dilution of normal rabbit serum (DakoCytomation) in TBS [50 mM Tris·HCl (pH 7.6), 150 mM NaCl] was applied to each slide for 5 min. Sections were incubated overnight at 4°C with one of the following primary mouse monoclonal antibodies in 0.1 ml TBS that contained 0.1% (wt/vol) BSA: anti-collagen type IV (3.13 μg/ml, Developmental Studies Hybridoma Bank at the University of Iowa, catalog no. M3F7), anti-K7 (1.1 μg/ml, catalog no. NCL-CK7-OVTL, Vision Biosystems/Novocastra, Norwell, MA), anti-K13 (1:20 dilution, catalog no. AB22685, Abcam), anti-K14 (0.5 μg/ml, catalog no. MCA890, Serotec, Raleigh, NC), anti-K17 (10 μg/ml, catalog no. C9179, Sigma), or anti-uroplakin III (1:50 dilution, mouse monoclonal IgG obtained from T. T. Sun, New York University School of Medicine). Slides were then rinsed three times with TBS and incubated with rabbit anti-mouse biotinylated secondary antibody (3.3 μg/ml, catalog no. E0354, DakoCytomation) at room temperature for 30 min, and rinsed three times again with TBS. StreptABComplex/

RIGHTSLINK www.physiology.org/journal/ajprenal by ${individualUser.givenNames} ${individualUser.surname} (037.055.225.009) on June 10, 2018.
Copyright © 2010 American Physiological Society. All rights reserved.

HRP (DakoCytomation) was added to slides and incubated for 30 min. Slides were rinsed twice with TBS, once with ultrapure water, and treated with 1× Enhanced DAB Metal Substrate solution (Pierce, Rockford, IL) for 15 min. After two more rinses with water, sections were counterstained with a 1:1 dilution of Gill's formula hematoxylin (Vector Laboratories, Burlingame, CA), then dehydrated by a series of ethanol and xylene substitute washes. Images were captured as described above.

In Vitro Propagation of Epithelial Cells from Bladder Exstrophy Specimens

Propagation of nonepithelial cell types was selected against by use of serum-free medium and Primaria coating of polystyrene culture flasks, as previously described (2). Resultant cultures were entirely epithelial cells and exhibited positive immunoreactivity with antibodies specific for keratin antigens. Cells were passaged with trypsin onto no. 1.5 glass coverslips (0.170 ± 0.003 mm in thickness) that housed a layer of silicone rubber that exhibited 1-cm^2 square openings to contain the culture.

Fluorescent Immunohistochemical Detection

A triple-labeling fluorescence protocol was used for Cy2- and Cy3-conjugated detection of cytokeratins and the hemidesmosome-indicating proteins laminin-5 (L5) and integrin-α-6 (IA6). Exstrophic cells were fixed in 4% paraformaldehyde at room temperature for 15 min, washed with PBST (0.05% Tween 20, catalog no. P-3563, Sigma), then permeabilized with 0.1% Triton X-100 in PBS for 5 min. Following washing in PBST, the first primary antibody (specific to K7, K13, or K14) was incubated for 1 h at room temperature. The cells were washed with PBST, then incubated at room temperature with the first secondary antibody (goat anti-mouse IgG conjugated to Cy2, 7.5 μg/ml, catalog no. 115-225-146, Jackson ImmunoResearch) for 30 min. Rinsing in PBST followed, then incubation with the second primary antibody, specific to L5 (1:100 dilution, rabbit monoclonal IgG_1 donated by Jonathan Jones at Northwestern University, Evanston, IL) or IA6 (50 μg/ml, catalog no. MAB1378, Chemicon, Temecula, CA) for 1 h. Following another washing with PBST, the cells were incubated with the second secondary antibody (goat anti-rabbit conjugated to Cy3, catalog no. 111-165-144, Jackson ImmunoResearch or goat anti-rat conjugated to Cy3, catalog no. 112-165-167, Jackson ImmunoResearch) for 30 min at room temperature. Washing in PBST followed, then incubation with Alexa Fluor 647 phalloidin (catalog no. A22287, Molecular Probes/Invitrogen) for 20 min. The slides were coverslipped with ProLong antifade media + DAPI (catalog no. P36931, Molecular Probes/Invitrogen). *Z*-stacks were taken with a DC500 camera mounted on a Leica DMI6000B using a ×63 oil objective (NA = 1.32) at image resolutions of 1,300 × 1,030 (6.7 μm/pixel). Out of plane light was removed via the Richardson-Lucy algorithm using Autoquant X2 deconvolution software (MediaCybernetics, Bethesda, MD). Colocalization analysis was performed by the JACoP plugin within ImageJ v1.37 software (NIH freeware, http://rsb.info.nih.gov/ij).

In Situ Hybridization

A pGEM3Zf(-) plasmid containing an insert encoding exon 8 of the mouse *FGFR2* gene was acquired from Dr. Andrew Farr (University of Washington, Seattle, WA). Subsequent dideoxy sequencing confirmed that the mouse sequence of this 148-bp insert differed from the human sequence at only three positions, thus validating the use of the mouse sequence as a probe for human specimens. The plasmid was linearized by *Eco*R1 and *Hind* III restriction enzymes for synthesizing sense and antisense probes, respectively. After digestion was confirmed by electrophoresis through a 1% (wt/vol) agarose gel, contaminants were removed through phenol/chloroform extraction. Purified insert cDNA was recovered by precipitation with ethanol and subsequent sedimentation. Sense and antisense single-stranded RNA probes were generated by SP6 or T7 RNA polymerase-catalyzed incorporation of digoxigenin (DIG) according to the manufacturer's instructions for a DIG RNA labeling kit (SP6/T7, catalog 11-175-025-910, Roche Applied Science). RNA-DIG probe concentrations were determined by dot blot analysis.

Sections for hybridization were dewaxed, rehydrated, treated with 100 μg ml^{-1} proteinase K for 10 min at 37°C, and subjected to prehybridization for 4 h at 58°C with a solution that contained 50% (vol/vol) deionized formamide, 4× SSC (where 1× = 150 mM NaCl and 15 mM sodium citrate at pH 7.0), 5% (wt/vol) dextran sulfate, 1× (vol/vol) Denhart's solution, 0.2 mg/ml salmon sperm DNA, and 100 units/ml RNase inhibitor. RNA-DIG probes were mixed into the prehybridization solution at a final concentration of 2 μg/ml, added to the sections, and hybridized for 15 h at 56°C. Unbound RNA-DIG probes were removed by a series of extensive washes with 2× SSC that contained 50% formamide (vol/vol) at 60°C followed by washes at ambient temperature with reducing concentrations of SSC (1, 0.25, 0.1, and 0.05×). Sections were blocked with blocking solution for 30 min and incubated for 1 h with an anti-DIG antibody coupled to alkaline phosphatase (1:200 dilution, 3.75 units/ml, catalog no. 11–093-274–910, Roche Applied Science). Immunoreactive signals were visualized by color development as described above.

Quantification of Immunoreactive Signals in Paraffin-Embedded Human Tissue Sections

Because the size of the bladder specimen was typically <1 cm^3, the quantity of useable tissue sections was rate-limiting, a constraint that resulted in lack of statistical power due to the absence of urothelium in some specimens. In all cases, however, it was obvious if the signal was absent, weak, moderate, or strong. A semiquantitative scoring system was implemented to record and classify the data. The legends to Tables 2 and 3 detail the key to our scoring system, which was tabulated by two blinded investigators.

Transgenic Mice

Procedures for the use of mice in this study were approved by the Institutional Animal Care and Use Committees of the University of Washington and Seattle Children's Hospital. Animals were maintained in a specific pathogen-free vivarium where food and water were available ad libitum. Genotyping was confirmed by *Taq* polymerization of genomic DNA annealed to exon-specific oligonucleotide primers and visualized by agarose electrophoretic gels stained with ethidium bromide.

Mice of the C57BL/6J strain that contained a targeted disruption to the *FGF7* gene were obtained from E. Fuchs (Rockefeller University) and bred to yield colonies of homozygous (−/−) mice (19, 20, 27). Erythematous skin and matted fur were noted in FGF7-null mice injected with rFGF-7, as previously noted (19).

C57BL/6J mice harboring a targeted disruption to the *FGF10* gene were a kind gift from A. Farr (University of Washington) and J. Rubin (National Cancer Institute) and bred to yield homozygous (−/−) mice that are stillborn due to a defective pulmonary system.

Histological Evaluation of Bladder Mucosa from FGF-10 (−/−) Mice

For FGF-10 (−/−) histological analysis, pups were obtained either via removal by caesarian sectioning or by removal from the uterus upon delivery. Pups were fixed in formalin, sectioned, and stained with Masson's trichrome.

Isolation and Characterization of Recombinant FGF-10

Recombinant (r) FGF-10 was isolated from *Escherichia coli* as previously described (2, 25). Preparations of rFGF-10 were quality controlled by SDS-PAGE, specific reactions with anti-FGF-10 IgGs,

RIGHTSLINK www.physiology.org/journal/ajprenal by ${individualUser.givenNames} ${individualUser.surname} (037.055.225.009) on June 10, 2018.
Copyright © 2010 American Physiological Society. All rights reserved.

Table 1. *Demographics of exstrophy subject population*

Specimen	Diagnosis	Surgery	Age	Sex
1	Classic exstrophy	NDA	NDA	NDA
2	Classic exstrophy; possible polyp	CPR	4 wk	M
3	Classic exstrophy	CPR	5 days	F
4	Classic exstrophy	PR	0 days	M
5	Classic exstrophy; possible polyp	R	7 mo	M
6	Classic exstrophy; polyp	PR	4 days	M
7	Classic exstrophy	PR	5 days	M

Tissue explants were taken during the stage of the surgery listed. NDA, no data available; CPR, complete primary repair; PR, primary repair; R, revision.

circular dichroism spectroscopy, endotoxin thresholds, and concentration-dependent stimulation of DNA synthesis (25). After the addition of heparin to a final concentration of 5 μg/ml, the complex of rFGF10 and heparin was dialyzed against vehicle [120 mM NaCl, 2.7 mM KCl, 4 mM NaH_2PO_4 (pH 7.4), 5 μg/ml heparin] overnight at 4°C. The solution was sterilized by passage through a 0.2-μm sterile filter into 1-ml aliquots that contained 270 μg and stored at −20°C.

Systemic Administration of Recombinant FGF-10 to Wild-Type and FGF-7 (−/−) Mice

Male animals weighed 25–29 g and were housed in our laboratory's vivarium. rFGF-10 (0.27 mg/ml in vehicle) or vehicle alone was administered daily via intraperitoneal injection into five wild-type C57BL/6J or five FGF-7 (−/−) mice for 14 days. All groups of animals tolerated intraperitoneal injections of rFGF-10 or vehicle without adverse effects. rFGF-10 was detected in the serum of wild-type and transgenic animals by Western immunoblot analyses with antibodies specific for the C-terminal region of rFGF-10.

Histological Evaluation of Urothelial Cell Layer Expansion

On *day 14* of growth factor administration, animals were euthanized and their genitourinary tracts were harvested en bloc and fixed in methyl Carnoy's solution. Representative cross sections of the left renal pelvis, ureter, bladder, prostatic urethra, membranous urethra, and anterior urethra were obtained at standardized locations using consistent anatomic landmarks and stained with hematoxylin and eosin, Masson's trichrome, and antibodies specific for Ki-67 (catalog no. NCL-Ki67-MM1, Novocastra). Urothelial expansion was measured by two blinded, independent investigators who counted cell layers. They concurrently averaged their individual counts obtained at the 12 o'clock, 3 o'clock, 6 o'clock, and 9 o'clock positions. Cells were counted if their nucleus crossed a straight line drawn perpendicular from the basal lamina toward the lumen. Separately, cell cycle progression was measured as either positive or negative by the appearance of positive Ki-67 cells within the specimen.

Statistical Analysis of Mouse rFGF-10 Experiments

The number of epithelial layers in each specimen was scored by two raters blinded to the mouse genotype (wild-type or FGF-7 −/−) and treatment group (vehicle alone or rFGF-10). Interrater reliability between the two raters' scores was assessed via an intraclass correlation coefficient and found to be very good (0.97 for bladder specimens). The two scores from different raters were then combined to obtain a single average score for each individual mouse. The average epithelial layering scores were then summarized with means and SD estimates. Two-sample Student's *t*-tests were used to assess the differences in epithelial layering between treatment groups. The impact of treatment with rFGF-10 was assessed separately in wild-type and in FGF-7 (−/−) mice.

RESULTS

Structure and Organization of von Brunn's Nests

Demographics of exstrophy patient population. Table 1 describes the demographics of exstrophy subjects whose bladder specimens exhibited von Brunn's nests and/or cystitis cystica. All subjects presented with classic exstrophy and underwent surgical repair at Seattle Children's Hospital.

Organization and characteristics of von Brunn's nests. von Brunn's nests were located within the superficial lamina propria of exstrophic bladders and exhibited a characteristic structure, which is illustrated in Fig. 1. The nests were observed to be a cyclic, polarized collection of cells gathered around a variably sized lumen. The number of cell layers in each nest was variable, but typically ranged from three to five.

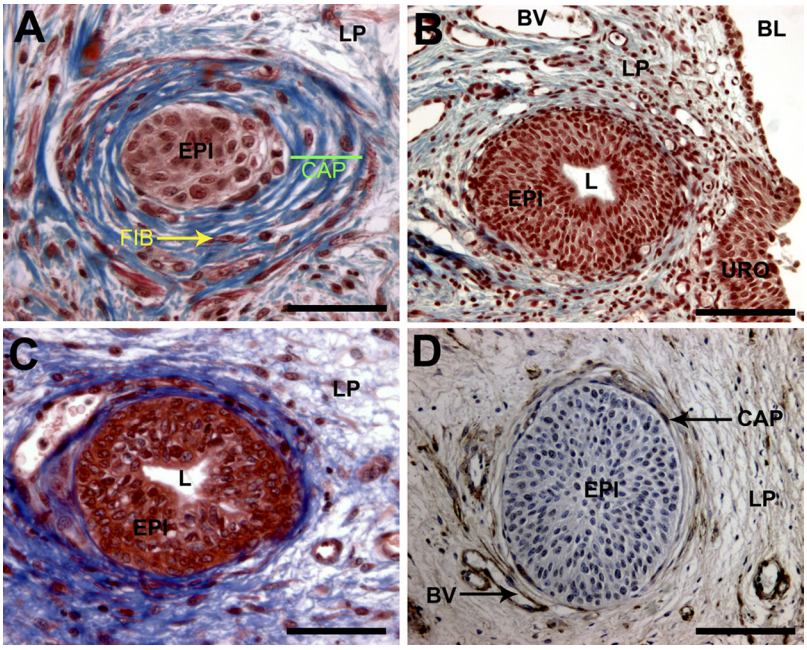

Fig. 1. Structure of von Brunn's nests in exstrophic bladder. *A–C*: Masson's trichrome stain. *D*: immunohistochemistry with antibodies specific for type IV collagen. *A* and *C*: bar = 50 μm, magnification = ×40. *B* and *D*: bar = 25 μm, magnification = ×20. EPI, epithelium; CAP, capsule of von Brunn's nest; FIB, fibroblast; L, lumen of von Brunn's nest; BL, lumen of bladder; LP, lamina propria; BV, blood vessel; URO, urothelium.

www.physiology.org/journal/ajprenal by ${individualUser.givenNames} ${individualUser.surname} (037.055.225.009) on June 10, 2018.
Copyright © 2010 American Physiological Society. All rights reserved.

Cells of the von Brunn's nests were surrounded by a collagen-rich shell. The presence of types I and III collagen fibrils was confirmed by microscopic visualization of Masson's trichrome-stained sections (Fig. 1, *A–C*). The presence of type IV collagen was confirmed by immunohistochemistry (Fig. 1*D*), where distinctive immunoreactive signals of brown color were observed within the shell. Such shells often failed to exhibit a sufficiently large aggregate of stroma to be formally classified as a capsule. The specificity of these anti-type IV collagen immunoglobulins was confirmed by positive immunoreactivity with the vascular extracellular matrix (arrow pointing to BV in Fig. 1*D*), a known site of type IV collagen synthesis and processing. The source of the collagen which comprises the capsule-like structure is the fibroblast (yellow arrow pointing to flattened cell in Fig. 1*A* and black arrow pointing to a flattened cell labeled CAP in Fig. 1*D*).

An organized basement membrane was observed to distinctly delineate the border between cells of the von Brunn's nest and the shell/capsule. Anchored to the basement membrane was a layer of basal cells with prominent nuclei. The remainder of the nest was observed to be occupied by several layers of cells which surrounded a lumen that varied in size. Cells of the von Brunn's nest were tightly packed together and exhibited an overall organization consistent with a polarized phenotype.

von Brunn's nests consistently exhibited a Masson's trichrome staining pattern, a type IV collagen-immunoreactive profile, and an overall cellular organization that were remarkably similar to

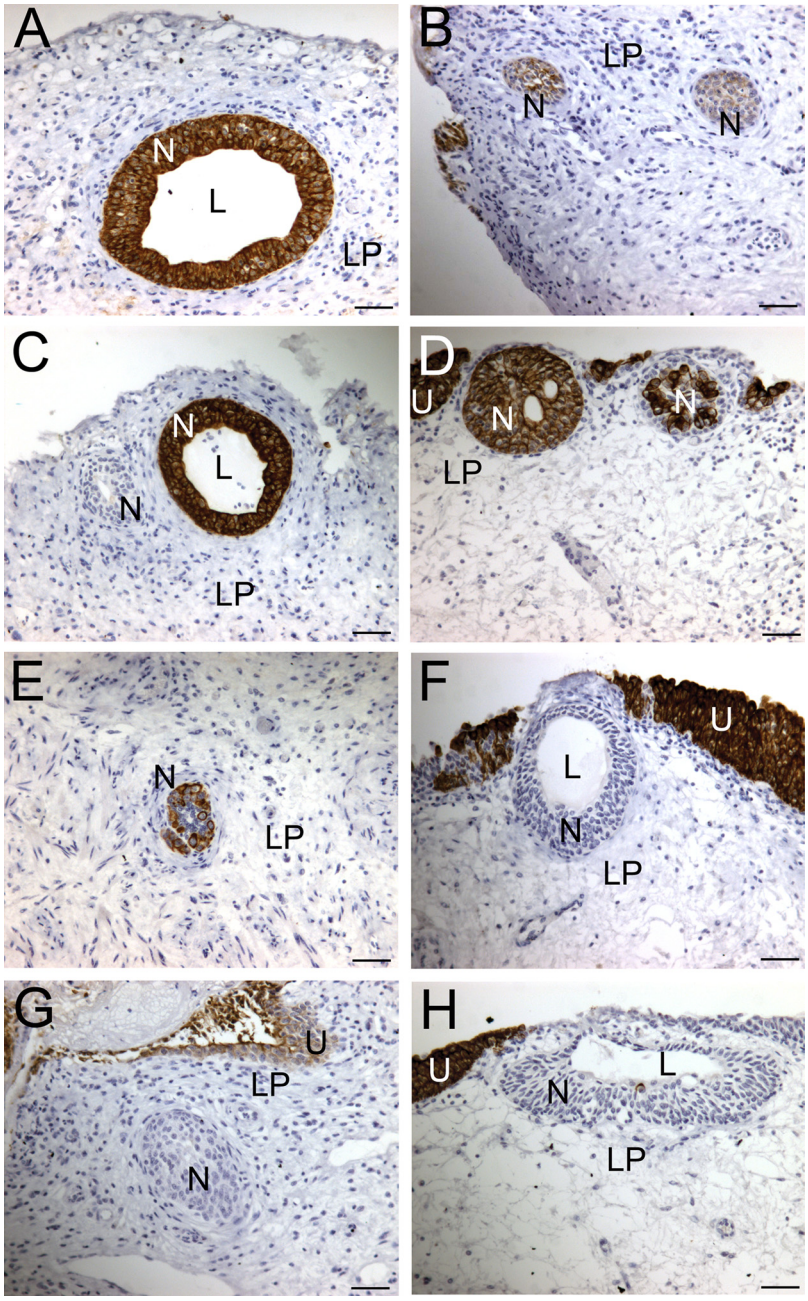

Fig. 2. K7 expression by cells of the von Brunn's nests defines the cells as epithelial. Shown are representative sections of bladder mucosa. Immunoreactive signals for K7 are indicated by the brown color. *A–H*: K7 antibody treatment. LP, lamina propria; N, von Brunn's nest; L, lumen; U, urothelium. Bar = 40 μm, magnification = ×20.

RIGHTSLINK www.physiology.org/journal/ajprenal by ${individualUser.givenNames} ${individualUser.surname} (037.055.225.009) on June 10, 2018.
Copyright © 2010 American Physiological Society. All rights reserved.

that of urothelial cells that comprise the transitional epithelial lining of the lower urinary tract (Fig. 1*B*). The collective evidence raised the question of the extent to which cells of the von Brunn's nest were derived from, or similar to, urothelial cells of transitional epithelium (urothelium) and whether nests were present in normal bladders.

K7 immunoreactivity defines cells of the von Brunn's nest as epithelial cells. K7, a type II keratin which typically couples with K19 in heterotypic keratin chains to form cytoplasmic intermediate filaments, was chosen to aid the classification of nested cells. K7 is recognized as an accepted marker of epithelial cells (31). Immunoreactive K7 signals were observed

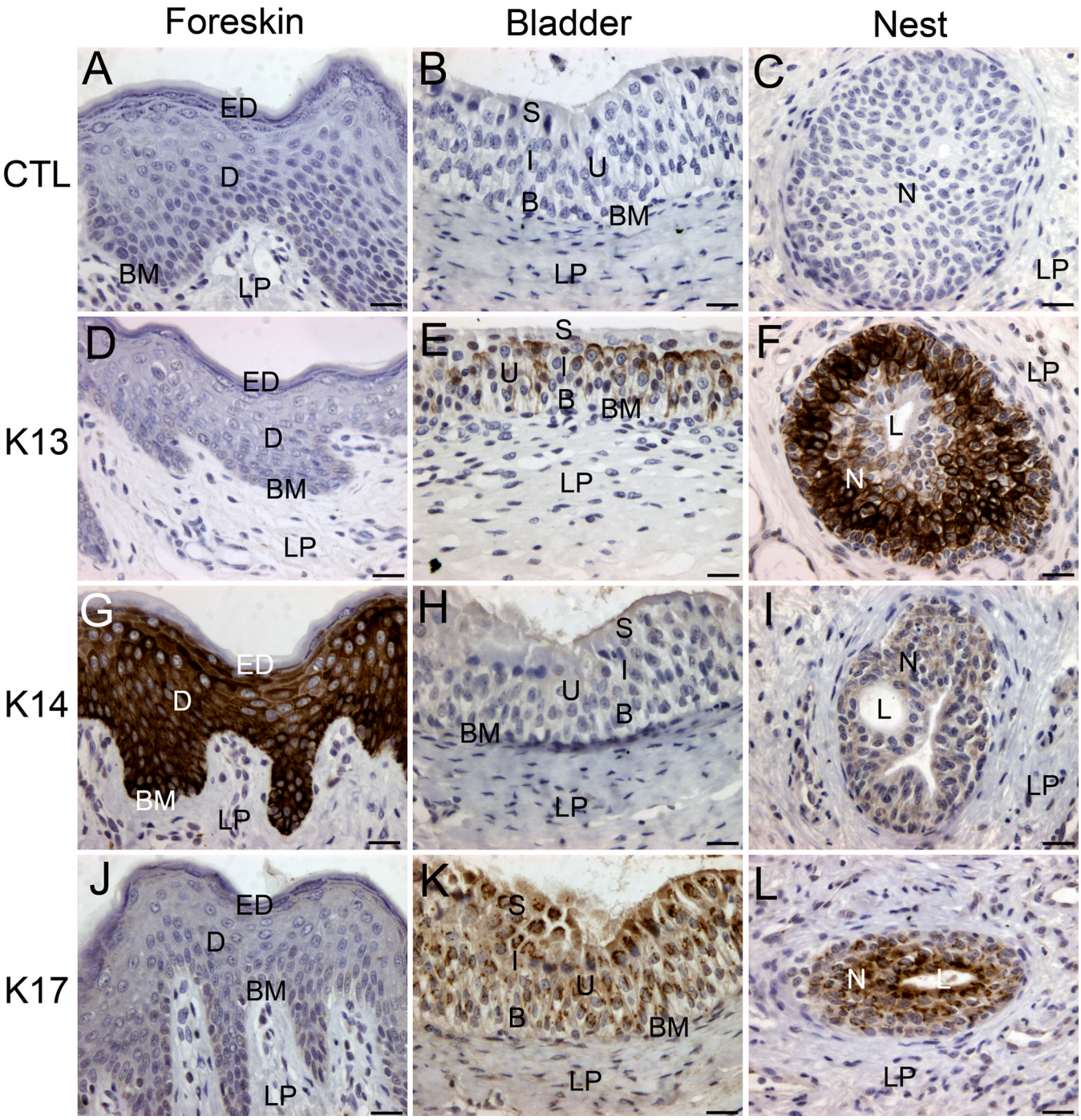

Fig. 3. Keratin profiling defines epithelial cells of the von Brunn's nest as transitional. Immunoreactive signals for K13, K14, and K17 are indicated by the brown color. *A–C*: no primary antibody control. *D–F*: K13 antibody treatment. *G–I*: K14 antibody treatment. *J–L*: K17 antibody treatment. *A*, *D*, *G*, and *J*: human foreskin. *B*, *E*, *H*, and *K*: human bladder mucosa. *C*, *F*, *I*, and *L*: representative von Brunn's nest. ED, epidermis; D, dermis; BM, basement membrane; LP, lamina propria; S, superficial layer; I, intermediate layer; B, basal layer; U, urothelium; N, von Brunn's nest; L, lumen of von Brunn's nest. Bar = 20 μm, magnification = ×40.

RIGHTSLINK www.physiology.org/journal/ajprenal by ${individualUser.givenNames} ${individualUser.surname} (037.055.225.009) on June 10, 2018.
Copyright © 2010 American Physiological Society. All rights reserved.

Table 2. *Scoring keratin immunoreactivity in exstrophic von Brunn's nests*

Specimen	K7	K13	K14	K17
1	+ + / + + + +	+ + / + + + +	−	+ +
2	+ + / + + + +	NDA	−	+ + / + + + +
3	+ + / + + + +	±	−	+ + / + + + +
		+ + / + + + +		
4	+ + + +	+ + / + + + +	−	+ + / + + + +
		+ +		
5	+ + + +	+ + + +	−	+ + / + + + +
6	+ + + +	+ + + +	−	+ +
7	+ + / + + + +	−	−	+ + / + + + +
		±		

Two scores indicated the signal intensity was variable. The K7 immunoreactivity pattern in *specimen 5* was patchy. −, negative. **±,** weak; **++,** moderate; **++/++++,** moderate to strong; **++++,** strong.

to fall within the following four types of patterns. In the first, there are consistently strong K7+ signals in every cell of the von Brunn's nest (Fig. 2, *A*, *C*, and *D*). In the second, weak K7+ signals are in every cell (Fig. 2*B*). In the third, strong K7+ signals are in variable patterns. In some von Brunn's nests, the basal layer of cells lacked detectable K7+ signals while the luminal layer exhibited strong K7+ signals (Fig. 2*D*, *right* nest). This pattern was also observed to be reversed, with basal cells exhibiting strong signals and the luminal cells being negative (Fig. 2*E*). In the fourth, von Brunn's nests were observed to be K7 negative (Fig. 2, *F–H*). This observed lack of immunoreactivity cannot be attributed to reagent failure because positive signals were obtained from control specimens included in every immunostaining procedure (not shown). Strong K7+ signals were also observed in urothelial cells of the same specimen and section that exhibited negative immunoreactivity in cells of the von Brunn's nest (Fig. 2*F*). Despite these patterns of variable immunoreactivity, sufficient data from numerous specimens and sections were obtained to classify cells of the von Brunn's nests as epithelial cells.

Epithelial cells of von Brunn's nests exhibit markers of transitional cell differentiation. Specific antibodies to recognized indicators of transitional (K13 and K17) and squamous differentiation (K14) (21, 44, 53) were used to determine the keratin profile of epithelial cells of the exstrophic bladder (Fig. 3). Nested cells exhibited weak to nil immunoreactive signals for K14 (Fig. 3*I*), indicating that epithelial cells of the nest were not undergoing squamous cell differentiation. Intense immunoreactive K14 signals were observed in human foreskin dermis (Fig. 3*G*), a positive control tissue well known to express K14 as part of its squamous differentiation program. Immunoreactive K14 signals in foreskin control tissue were absent in nuclei but strong in cytoplasm, in agreement with the known location of cytokeratin-containing intermediate filaments. In contrast, weak to nil immunoreactive K14 signals were observed in bladder transitional epithelia obtained from vesicoureteral reflux surgical explants, which served as a negative control (Fig. 3*H*) due to its normal phenotype (17).

K17 is an accepted marker of normal transitional epithelia (45). Moderate to strong immunoreactive K17 signals were observed within cells of the von Brunn's nest (Fig. 3*L*). Nuclei were devoid of signals. A polarized distribution was observed, with moderate signals within cells that adhere to an underlying connective tissue capsule and strong signals within cells that line the lumen of the von Brunn's nest (Fig. 3*L*). In normal transitional epithelia (Fig. 3*K*), which served as a positive control tissue, observed signals were intense and distributed in a focal, punctate pattern in a manner consistent with that of intermediate filaments. The negative control tissue, dermis from human foreskin, was negative for K17 (Fig. 3*J*).

To further confirm the transitional subtype, immunostaining specific to K13 antigens was performed. The basal and intermediate cell layers of the von Brunn's nests were observed to exhibit positive signals, while the superficial cells showed weak to no signal (Fig. 3*F*). Urothelium from normal bladder served as the positive control, displaying signals within the cytoplasm of basal and intermediate cells (Fig. 3*E*). The lack of expression of K13 in the superficial urothelial layer of normal bladder confirms a prior report where expression was limited to the basal and intermediate cell layers (30). Squamous epithelium of the human foreskin dermis served as a negative control, exhibiting weak to nil K13 signals (Fig. 3*D*).

The collective data from the seven exstrophy specimens were assembled, scored, and subjected to semiquantitative analysis. It was straightforward to classify the immunoreactive signals of a specimen as negative, weak, moderate, moderate-to-strong, or strong. The relative steady-state levels of immunoreactive signals for K7, K13, K14, and K17 from all von Brunn's nest specimens are summarized in Table 2. K7 was the keratin tested that consistently exhibited the strongest immunoreactive signals, so much so that we routinely use it as a positive control marker in immunohistochemical assays. K17 also exhibited signals that were consistently strong. Positive signals for K13 were variable and described by a range of signals from weak to strong. In marked contrast, immunoreactive K14 signals were absent

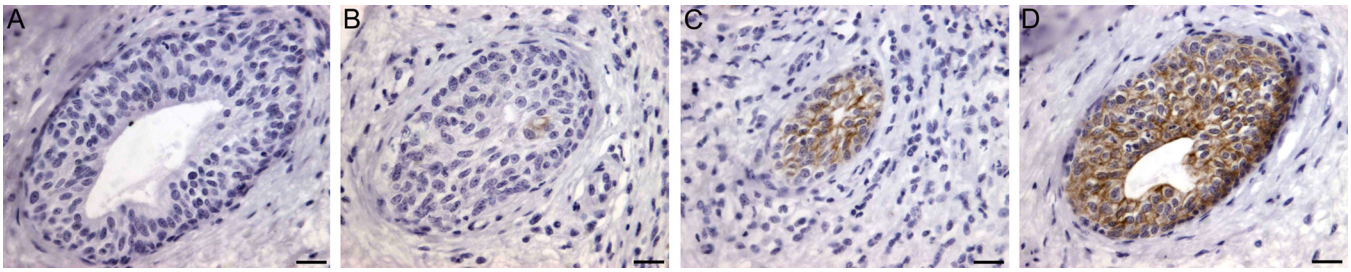

Fig. 4. K7 is a potential marker of von Brunn's nest maturation in the exstrophic bladder. Shown are immunoreactive signals from a mouse monoclonal IgG specific for K7 (brown). Sections were counterstained with hematoxylin. Shown is immunohistochemistry of the different morphological stages (*B–D*) of Von Brunn's nest in the same tissue section; *A* is the negative control. *B–D*: expression of K7 as a function of the morphology of von Brunn's nests. Bar = 20 μm, magnification = ×40.

RIGHTSLINK www.physiology.org/journal/ajprenal by ${individualUser.givenNames} ${individualUser.surname} (037.055.225.009) on June 10, 2018.
Copyright © 2010 American Physiological Society. All rights reserved.

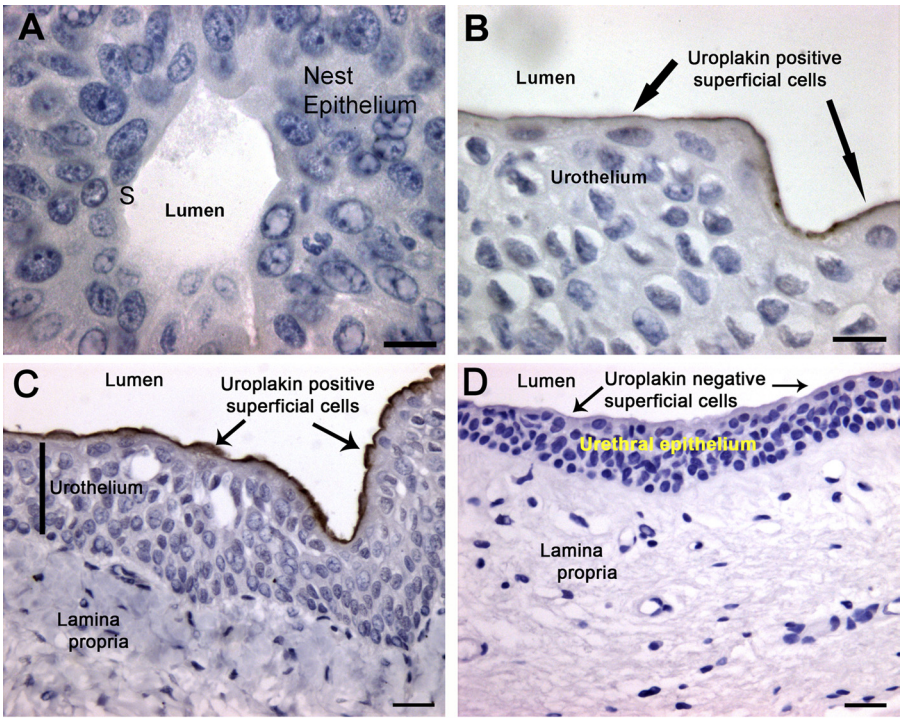

Fig. 5. The superficial layer of von Brunn's nest epithelial tissue does not express uroplakin IIIb. Immunoreactive signals for uroplakin IIIb are indicated by the brown color. Specimens were counterstained with hematoxylin (blue). *A*: superficial layer and lumen of von Brunn's nest. Note the lack of signal in the superficial cell layer. N, von Brunn's nest; S, superficial cell layer. Bar = 10 μm, magnification = ×100. *B*: normal human bladder positive control specimen. Bar = 10 μm, magnification = ×100. *C*: normal human ureter positive control specimen. Bar = 20 μm, magnification = ×40. *D*: normal anterior urethra from adult male specimen. Bar = 20 μm, magnification = ×40.

in all von Brunn's nests observed. Many, if not all, of the specimens exhibited numerous instances where histological and immunological features were well preserved across adjacent sections.

Keratin 7 presence is associated with von Brunn's nest maturation. The keratin profile of the mature von Brunn's nest has been described in Figs. 2 and 3. Close examination, however, of an exstrophic tissue specimen with multiple nests revealed an interesting observation. Figure 4 shows K7 immunostaining of von Brunn's nests within the specimen. Note the increasing size of the lumen in Fig. 4, *B–D*. We observed changes in K7 expression as the size of the von Brunn's nest's lumen changed in size. Figure 4*B* shows a nest with a very small lumen, exhibiting little to no K7 signal. In a nest with a slightly larger lumen, moderate K7 expression was apparent (Fig. 4*C*). With a large lumen, strong positive signals were observed (Fig. 4*D*).

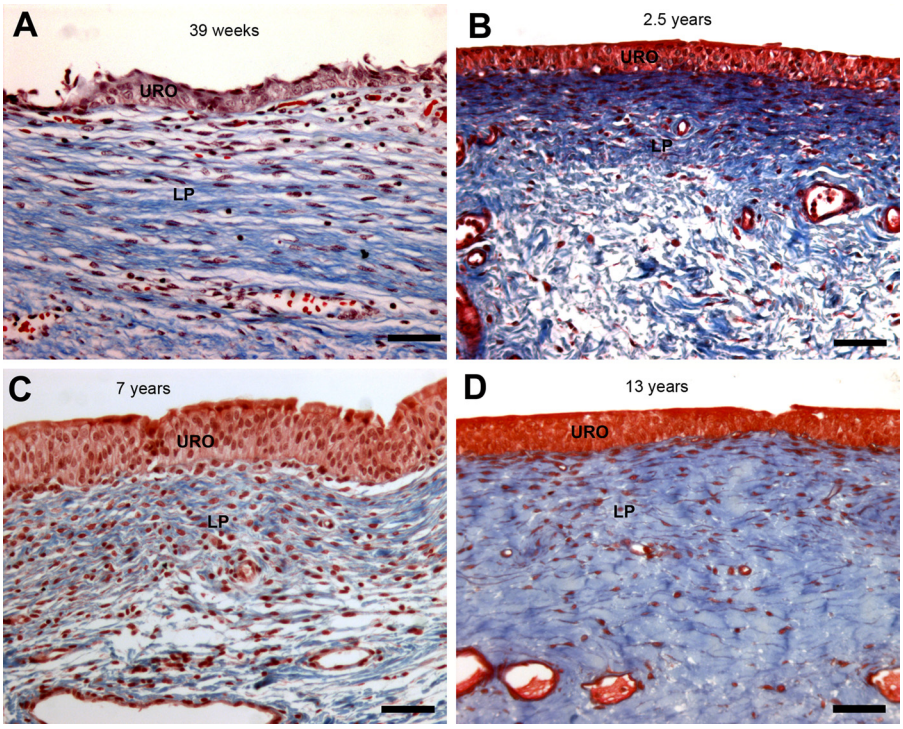

Fig. 6. von Brunn's nests are absent in normal bladder. Shown are Masson's trichrome-stained sections of formalin-fixed, paraffin-embedded bladder mucosa. *A*: normal bladder mucosa from 39-wk-old fetus. *B*: normal bladder mucosa from 2.5-yr female. *C*: normal bladder mucosa from 7-yr-old female. *D*: bladder mucosa from 13-yr-old male. LP, lamina propria; URO, urothelium. Bar = 50 μm, magnification = ×20.

RIGHTSLINK
www.physiology.org/journal/ajprenal by ${individualUser.givenNames} ${individualUser.surname} (037.055.225.009) on June 10, 2018.
Copyright © 2010 American Physiological Society. All rights reserved.

This pattern of data did not extend in a meaningful way to the analysis of other exstrophic bladder specimens. The pattern of data, however, does provide evidence that a subset of bladder exstrophy patients harbor von Brunn's nests whose development into larger nested structures can be tracked by monitoring of the relative steady-state expression levels for K7.

von Brunn's nests lack epitopes for uroplakin IIIb. Uroplakin IIIb comprises part of the asymmetrical unit membrane that uniquely covers the apical epithelial membrane of the mammalian lower urinary tract. It is therefore a useful marker for the terminal differentiation of transitional epithelium (13). There were no immunoreactive uroplakin IIIb signals for the superficial layer of von Brunn's nests (Fig. 5*A*), nor was it observed elsewhere in the nested tissue. In contrast, the uroplakin IIIb-specific antibodies exhibited the canonical superficial staining pattern for normal bladder (Fig. 5*B*) and ureteric (Fig. 5*C*) urothelium.

Epithelium from the male anterior urethra failed to react with uroplakin IIIb antibodies (Fig. 5*D*), thus serving as a negative control. The lack of uroplakin IIIb-immunoreactive signals in the superficial layer of the male anterior urethra suggests that this epithelium *1*) is developmentally distinct from transitional epithelium of the bladder and urethra and *2*) should not be referred to as urothelium.

von Brunn's Nests are Absent in Normal Pediatric Bladders

Representative data of normal bladder mucosal specimens stained with Masson's trichrome are shown in Fig. 6. The four human specimens examined did not contain von Brunn's nests. A representative 39-wk fetal specimen displayed a developing urothelium, consistent with the young age of the fetus, and a lamina propria that was devoid of nests (Fig. 6*A*). The specimens from a 2.5-yr-old female, a 7-yr-old female, and a 13-yr-old male exhibited a normal mucosa which lacked detectable nest features (Fig. 6, *B*, *C*, and *D*, respectively). Within our collection of pediatric bladder biopsies, only bladder exstrophy specimens exhibited von Brunn's nests. Twenty-eight normal specimens, obtained over a 10-yr period as surgical explants from subjects undergoing repair for vesicourethral reflux (17), were clearly devoid of von Brunn's nests. The collective data indicate that the presence of von Brunn's nests in pediatric bladders is a functional consequence of an abnormal developmental program.

Developmental Defects in Mice: Does a Model of Bladder Exstrophy Exist?

No single gene has been identified to causally relate to bladder exstrophy (26). One such candidate is the *FGF10* gene

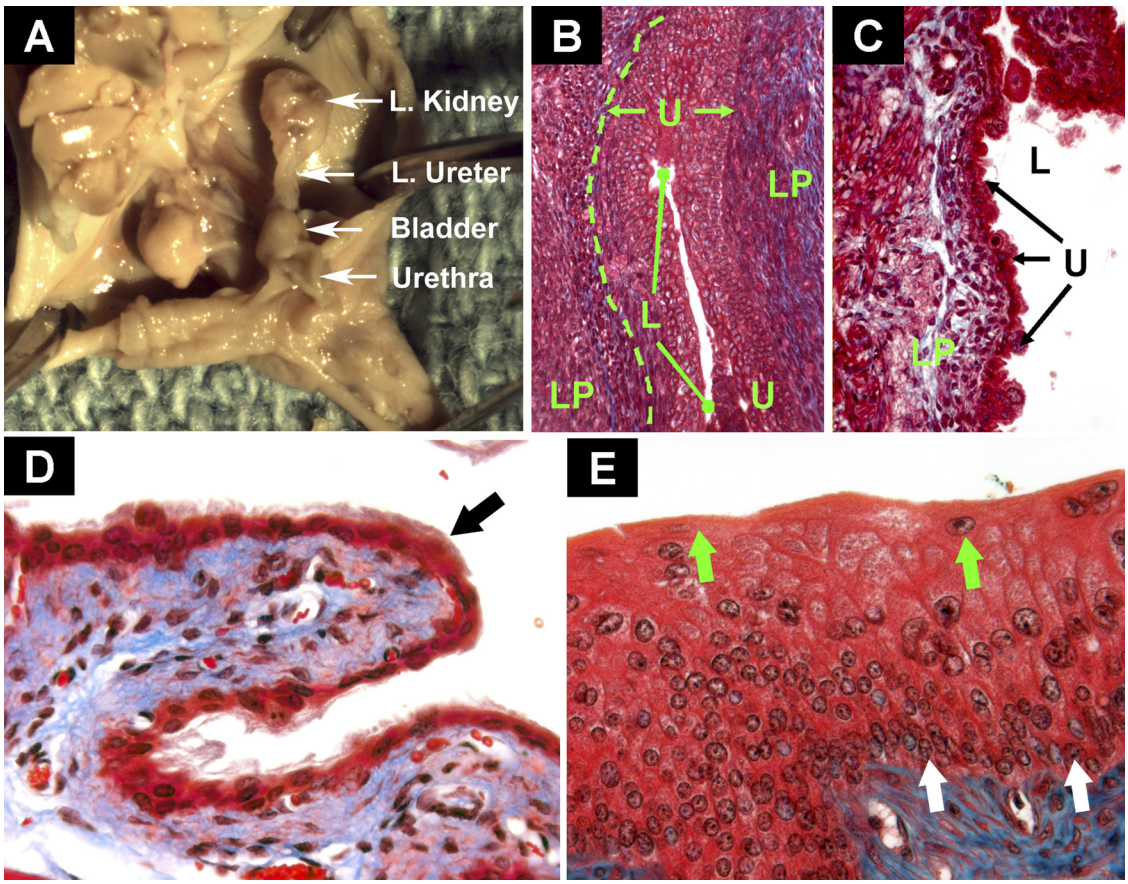

Fig. 7. FGF-10 (−/−) mice exhibit an abnormal urothelium but do not develop von Brunn's nests or exstrophy. *A*: gross anatomy of (−/−) urinary tract. Shown is dissection of (−/−) pup at 19 days postconception (*E17.5*, Theiler stage 27). *B*: histology of (+/+) bladder urothelium. Shown is Masson's trichrome stain of wild-type bladder mucosa. U, urothelium; LP, lamina propria; L, lumen; dotted line, basement membrane. *C*: histology of (−/−) bladder urothelium. Shown is Masson's trichrome stain of bladder mucosa. *D* and *E*: systemic administration of FGF-10 rescues abnormal urothelium of FGF-7 (−/−) mice. Bladder was stained with Masson's trichrome: mesenchymal collagen (blue) and epithelium (red). *D*: daily injection of vehicle for 14 days. Black arrow, abnormal urothelium. *E*: FGF-10 injection (5 mg/kg) for 14 days. White arrows, responsive basal cells in cell cycle; green arrows, restoration of superficial cell layer.

RIGHTSLINK www.physiology.org/journal/ajprenal by ${individualUser.givenNames} ${individualUser.surname} (037.055.225.009) on June 10, 2018.
Copyright © 2010 American Physiological Society. All rights reserved.

because FGF-10 (−/−) mice exhibit hypospadias (57), urorectal malformations (16), and the abnormal development of both limb buds and lungs (29). To determine whether the targeted disruption of the *FGF10* gene resulted in bladder exstrophy, pregnant female (+/−) mice were monitored for delivery of newborn pups, which were collected immediately and fixed with formalin. While there was no evidence of bladder exstrophy in this strain, gross anatomic inspection revealed that the left kidney and left ureter were either absent or dilated in two of three FGF-10 (−/−) pups (Fig. 7*A*). In all three FGF-10 (−/−) pups examined, the bladder and urethra were judged to be intact from a gross anatomic perspective.

Histologically, FGF-10 (−/−) bladders exhibited incomplete stratification of transitional epithelia (Fig. 7*C*). Basal and intermediate urothelial cell layers were consistently absent or diminished. The superficial urothelial layer was excessively swollen and displayed altered cytoplasmic:nuclear ratios, in a manner consistent with the absence of paracrine mediators of urothelial cell proliferation and differentiation (2, 49). There was no evidence of von Brunn's nests in the bladder lamina propria of FGF-10 (−/−) mice. This observation is consistent with the view that FGF-10 does not play an integral role in the cloacal membrane during embryogenesis in animal models. Patients with exstrophy rarely have limb anomalies or renal anomalies, and, by definition, do not have hypospadias.

Rescue of abnormal phenotype of FGF-7 (−/−) bladders by rFGF-10. Our finding of an undeveloped bladder urothelium in FGF-10 (−/−) mice is in agreement with the features of an underdeveloped urothelium in FGF-7 (−/−) mice (Fig. 7*D*, black arrow). The urothelium of FGF-7 (−/−) mice are known to lack intermediate cells, as assessed by electron microscopy and fluorescent immunohistochemistry (49). Unlike the FGF-7 (−/−) mice which are fertile, FGF-10 (−/−) mice are stillborn due to the lack of lungs. Since these two growth factors are conserved in terms of primary structure (4), paracrine mitogenic activity (2, 58) and interaction with the same tyrosine-kinase cell surface receptor (58), we elected to determine the extent to which rFGF-10 would stimulate urothelial cell cycle progression and stratification in two groups of mice: a wild-type C57BL/6J group and a FGF-7 (−/−) group of the same C57BL/6J strain.

Our preparations of rFGF-10 were able to rescue the undeveloped urothelium of FGF-7 (−/−) mice via the FGF-10 receptor pathway (Fig. 7*E*, white arrow). The mean number of cell layers in wild-type and FGF-7 (−/−) mice increased from 3.0 ± 0 and 2.3 ± 0.5, respectively, for injection of vehicle, to 7.2 ± 0.7 ($P = 0.038$) and 6.8 ± 1.3 ($P = 0.006$), respectively, for injection of rFGF-10. The mechanism underlying the observed expansion in mean cell layers was due to FGF10-dependent cell-cycle progression, as documented by immunostaining with anti-Ki67 antibodies. The percentage of specimens staining positive for Ki-67 ($n = 5$) was observed to increase from 0.0 (vehicle) to 0.2 (rFGF-10). The collective evidence from this 2-wk course of FGF-10 therapy demonstrates that *1*) the urothelium of wild-type mice undergoes a threefold expansion in the number of cell layers; *2*) an intact layer of plump, healthy superficial cells was restored to the abnormal urothelium of FGF-7 (−/−) mice (Fig. 7*E*, green arrow); and *3*) the FGF-10 receptor remains functional in FGF-7 (−/−) mice.

FGF-10 Signals Development of von Brunn's Nests in the Exstrophic Bladder

Localization of FGF-10 and its receptor to cells of the von Brunn's nest and the lamina propria. The positive finding that epithelial cells of the von Brunn's nest exhibit markers of metabolic pathways that contribute to transitional cell differentiation (K13 and K17, Fig. 3, *F* and *L*, respectively) led us to hypothesize that nested cells would express markers of pathways involved in the proliferation of basal urothelial cells of transitional epithelia. One such pathway is the paracrine network of FGF-10, its tyrosine kinase cell-surface receptor, and an undefined nuclear receptor, which are known to operate

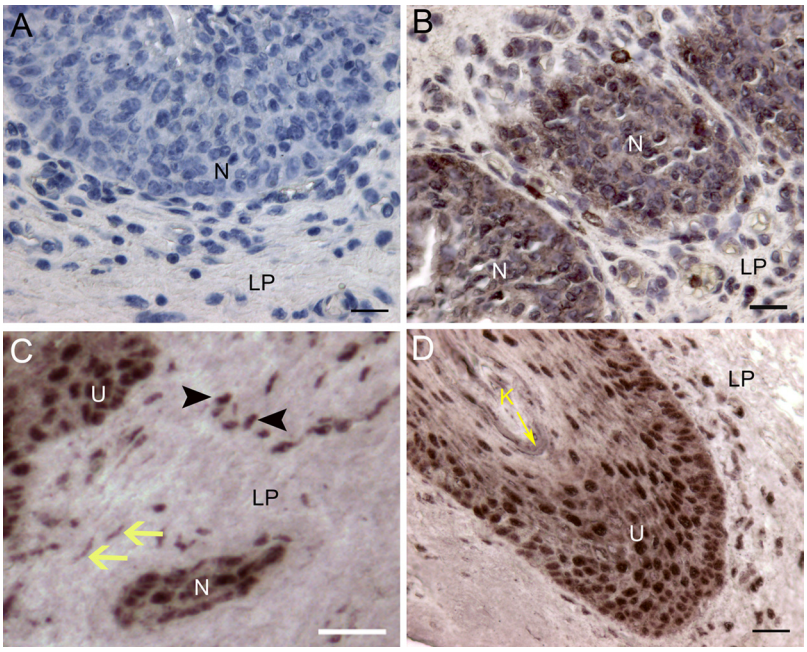

Fig. 8. Immunoreactive FGF-10 is detected in von Brunn's nests, in cells of the lamina propria, and in the urothelium of the exstrophic bladder. Shown are immunoreactive signals from a mouse monoclonal IgG specific for FGF-10 (brown). Section in *A* and *B* are counterstained with hematoxylin. *A*: no primary antibody control. *D*: exstrophic bladder urothelium. *A*, *B*, and *D*: bar = 20 μm; magnification = ×40. *C*: bar = 20 μm, magnification = ×20. N, nest; LP, lamina propria; U, urothelium. Arrowheads, round cell in lamina propria immunopositive for FGF-10. Yellow arrows, fibroblast immunopositive for FGF-10. Yellow K, keratinization.

RIGHTSLINK www.physiology.org/journal/ajprenal by ${individualUser.givenNames} ${individualUser.surname} (037.055.225.009) on June 10, 2018.
Copyright © 2010 American Physiological Society. All rights reserved.

within urothelial cells, as described in our prior reports (2, 25, 27, 58).

Strong immunoreactive signals for FGF-10 were observed within nested cells of the exstrophic bladder (Fig. 8, *B* and *C*; Table 3). Cells positive for FGF-10 are termed here as 10p cells. The presence of FGF-10 immunoreactive signals appeared to be independent of whether a von Brunn's nest exhibited a lumen or not. The basal, intermediate, and superficial cell layers of the von Brunn's nest all exhibited strong immunoreactive signals for FGF-10. Within individual cells, strong signals were observed in both the cytoplasm and nuclei, although, on occasion, nest nuclei failed to exhibit FGF-10 immunoreactivity.

Additionally, some cells of the lamina propria adjacent to the Brunn's nest exhibited strong FGF-10 signals (Fig. 8*C*). These FGF-10-positive cells were observed throughout the lamina propria. It was straightforward to classify them into two types. The first cell type was identified as the fibroblast (yellow arrows in Fig. 8*C*) according to three criteria: *1*) spindle-shaped cellular morphology, *2*) correlation with the blue-stained fibrillar collagen (type I or III) in Masson's trichrome-stained sections (Fig. 1), and *3*) synthesis of FGF-10, an observation in agreement with our prior reports (2, 25, 27, 58).

The second cell type was consistently observed to exhibit a rounded morphotype, a large immunopositive nucleus, and a small cytoplasm (black arrowheads, Fig. 8*C*). The identity and etiology of this second type of FGF-10-positive cells in the human bladder lamina propria are currently unknown.

Strong immunoreactive signals for FGF-10 were consistently observed in exstrophic bladder urothelium (Fig. 8*D*; Table 3), an observation in agreement with prior studies of normal bladder (2, 58). The source of FGF-10 synthesis, however, is not epithelial. Instead, the growth factor is synthesized by fibroblasts of the lamina propria and transported by a paracrine pathway into the urothelium (2, 58). In parallel experiments, in situ hybridization assays detected FGF-10 mRNA only in fibroblasts of the lamina propria; signals were absent in nest cells (not shown). It is in these fibroblasts that immunoreactive FGF-10 signals were detected (yellow arrow in Fig. 8*C*), a finding that supports the growth factor's synthesis in fibroblasts and paracrine transport into either urothelial cells or von Brunn's nests.

Strong immunoreactive signals for the FGF-10 receptor were also observed within nested cells (Fig. 9*B*). Much like its FGF-10 ligand, the observation of immunoreactive signals for the FGF-10 receptor appeared to be independent of whether a von Brunn's nest exhibited a lumen or not. All cell layers of the von Brunn's nest exhibited immunoreactive signals for the FGF-10 receptor (Fig. 9*B*). The nest epithelium exhibited two patterns of polarized immunoreactive signals for the FGF-10 receptor: *1*) apical distribution within the cells of the luminal, or superficial, layer and *2*) distribution in the basal layer in a

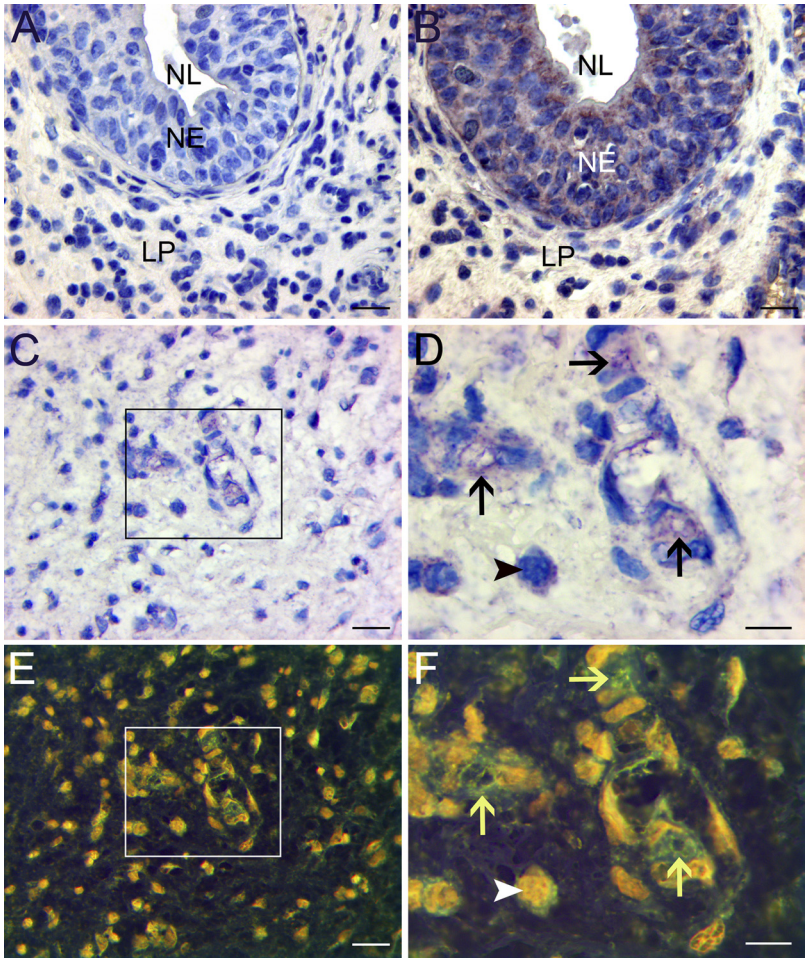

Fig. 9. FGF-10 receptor is a marker for the earliest stages of von Brunn's nest development in the exstrophic bladder. Shown are immunoreactive signals from a mouse monoclonal IgG specific for the FGF-10 receptor (*B–D*: brown/purple; *E* and *F*: green). Sections counterstained with hematoxylin (*A–D*: blue; *E* and *F*: gold). *A*: no primary antibody control. *B–F*: antibody treatment. NE, nest epithelium; NL, nest lumen; LP, lamina propria *A–C* and *E*: bar = 20 μm, magnification = ×40. *D* and *F*: bar = 10 μm, magnification = ×100. *Insets* in *C* and *E* correspond to *D* and *F*, respectively. Rp, receptor positive. Arrowheads in *D* and *F*, Rp single cell; arrows in *D* and *F*, Rp cell cluster. *E* and *F*: to better distinguish the hematoxylin blue color with the brown/purple color of the diformazan precipitate (corresponding to receptor signals), raw images of *C* and *D* were processed as follows: *1*) color intensity and luminance adjusted to 200 with Match Color tool of Photoshop, yielding *C* and *D*; *2*) resized with bicubic resampling to match the resolution of *A* and *B*; *3*) image inversion; and *4*) color intensity and luminance adjusted to 200, yielding *E* and *F*.

RIGHTSLINK www.physiology.org/journal/ajprenal by ${individualUser.givenNames} ${individualUser.surname} (037.055.225.009) on June 10, 2018.
Copyright © 2010 American Physiological Society. All rights reserved.

manner suggestive of a functional interface with the underlying type IV collagen capsule. In this specimen from a 4-wk-old male, a layer of keratin sits atop the apical plasma membranes of the superficial cell layer (Fig. 9*B*) in a manner that suggests that the FGF-10 mitogenic pathway is active in these nests. It is noteworthy that keratinization of the superficial layer occurred in both von Brunn's nests (Fig. 9*B*) and the urothelium (Fig. 8*D*) in specimens from the same patient.

Immunoreactive signals for FGF-10 receptor protein also localized to cells of the lamina propria (Fig. 9, *C–F*). Cells positive for the FGF-10 receptor are termed Rp cells. Interestingly, the unknown cell type that exhibited immunoreactive signals for FGF-10 (Fig. 8*C*, black arrowhead) also exhibited immunoreactive signals for the FGF-10 receptor (Fig. 9*D*, black arrowhead, and Fig. 9*E*, white arrowhead), indicating a role for these submucosal cells in the etiology and development of von Brunn's nests. It is hypothesized that two types of FGF-10 positive (10p) cells exist in the lamina propria of exstrophic bladders: 10pF, the canonical fibroblast that synthesizes FGF-10 but not the FGF-10 receptor, and 10pRp, the unknown cell type that is positive for both FGF-10 and the FGF-10 receptor.

10pRp clusters are potential precursors to von Brunn's nests. We also noticed that some of the cells that exhibited immunoreactive signals for the FGF-10 receptor gathered together to form clusters within the lamina propria (black arrows in Fig. 9*D* and yellow arrows in Fig. 9*F*). These clusters consisted of only a few cells and contained both 10pF and 10pRp cells. We felt it would be of importance to classify the relationship between these clusters found in the lamina propria and the cells of the von Brunn's nest.

To explore this relationship, the distribution pattern of the FGF-10 receptor-positive signaling cells was further examined by in situ hybridization assays to detect the mRNA encoding the FGF-10 receptor (Fig. 10). In the normal area (nonproximal to a Brunn's nest) of the lamina propria, overall cell density was considerably much lower than in areas of the lamina propria proximal to a nest. Most cells were identified as spindle-shaped fibroblasts. As observed previously (58) in normal tissues, fibroblasts did not hybridize to the antisense probe for receptor mRNA (Fig. 10*A*). In the area surrounding von Brunn's nests where overall cell density was high and spindle-shaped fibroblasts were infrequent, many cells exhibited positive signals for the FGF-10 receptor RNA probe (Fig. 10, *B–D*). Additionally, clustered cells exhibited strong hybridization signals for receptor RNA (Fig. 10, *B–D*, black arrows). Interestingly, these clusters were more frequently distributed in areas proximal to blood vessels (Fig. 11). Furthermore, positive round cells with large positive nuclei were found adjacent to blood vessels (Fig. 11*A*) or were intravascular (Fig. 11, *B*, *D*, *E*, and *F*), indicating a possible source of these cells. The presence of the FGF-10 receptor mRNA, in addition to the

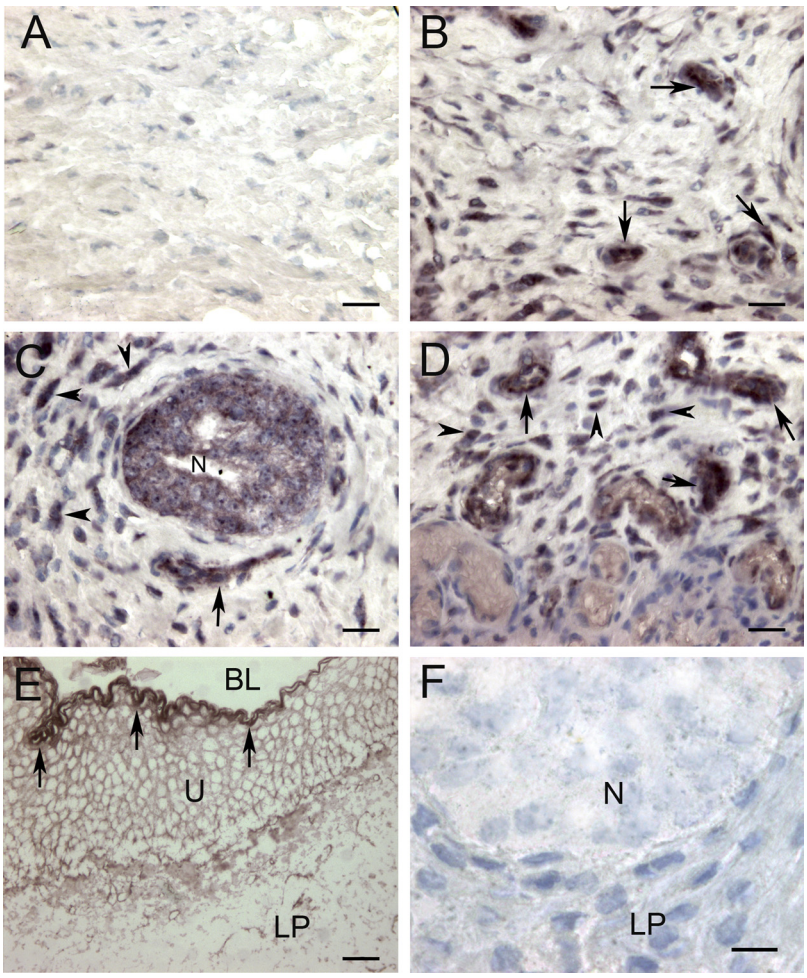

Fig. 10. Multiple sites of mRNA synthesis of the FGF-10 receptor in the exstrophic bladder. Shown are in situ hybridization antisense signals (dark brown in *A–E*) derived from an RNA probe complementary for receptor mRNA. *A*: region of the lamina propria devoid of von Brunn's nests. *B–D*: region of the lamina propria that is rich in von Brunn's nests; arrows point to the clusters formed by FGF-10 receptor mRNA-positive cells; arrowheads point to single positive cells. *E*: exstrophic bladder urothelium. U, urothelium, LP, lamina propria; arrows point to intense signals at a squamous keratinized epithelial cell layer that lines the bladder lumen (BL). *F*: sense signals from a region of the lamina propria that is rich in von Brunn's nest. All sections except *E* were counterstained with hematoxylin. N, nest epithelium. *A–E*: bar = 20 μm, magnification = ×40. *F*: bar = 10 μm, magnification = ×100.

RIGHTSLINK www.physiology.org/journal/ajprenal by ${individualUser.givenNames} ${individualUser.surname} (037.055.225.009) on June 10, 2018.
Copyright © 2010 American Physiological Society. All rights reserved.

cluster-forming ability of these cells and their high frequency in areas adjacent to nests, suggests that the 10pRp cells may have the potential to progress to von Brunn's nests.

Are von Brunn's nests derived from urothelial cells of transitional epithelium? Two types of structures function to anchor basal urothelial cells to their underlying basement membrane: the focal adhesion complex and the hemidesmosome. Because the existence of epithelial podosomes has recently been established (47, 48), we sought to determine the extent to which hemidesmosomes would be uniquely preserved in exstrophic epithelial cells propagated in vitro.

A normal in vitro keratin immunostaining pattern was observed as a diffuse network of intermediate filaments (Bassuk JA and Leaf EM, unpublished observations). Such a normal pattern was also observed in a subset of exstrophy specimens, as illustrated in Fig. 12*A*. Immunoreactive K14 signals were distributed throughout the cytoplasm in a manner consistent with the literature's description for "cytokeratins." Epithelial cells that expressed the normal keratin phenotype also synthesized and polymerized F-actin filaments into a cortical actin cytoskeleton, which was organized just beneath the plasma membrane (Fig. 12*A*).

Abnormal in vitro keratin immunostaining patterns were evident in a subset of exstrophy specimens. The following three types of abnormal patterns were observed by widefield fluorescence microscopy: *1*) foci of intense keratin signals (yellow arrow in Fig. 12*C*) that formed a dome atop the nucleus; *2*) foci of punctuate keratin signals (dotted yellow ellipse in Fig. 12*D*); and *3*) large islands of intense K7 immunoreactivity (white arrows in Fig. 12, *C* and *D*). Such islands, which were not observed in normal cells, were found at the periphery of cells and frequently corresponded to rounded structures identified by differential interference contrast microscopy (white arrows in Fig. 12*B*). These abnormal immunoreactive keratin signals appeared to be withdrawn from the central region of the cell in a manner which would preclude interaction of some intermediate filaments with the nucleus.

The abnormal islands of immunoreactive keratin signals exhibited a diameter of ~5–10 μm, which is similar to the hemidesmosome-containing podosome-like structure previously identified in adhering epithelial cells that include transitional cells (22, 47, 48). We hypothesized that these abnormal islands were the result of improperly functioning

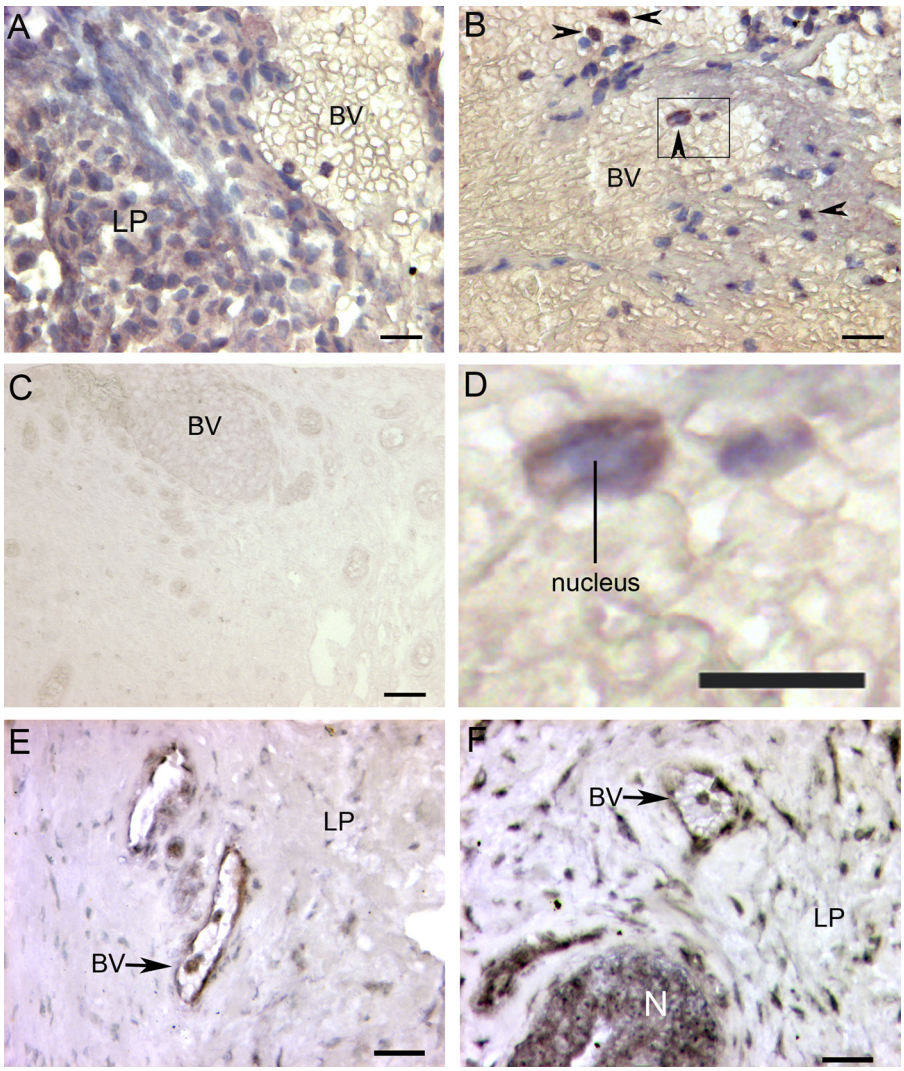

Fig. 11. Association of FGF-10 receptor mRNA synthesis with blood vessels of the exstrophic bladder. Shown are in situ hybridization signals (brown) derived from annealing of a specific RNA probe to receptor mRNA. All sections except *C* were counterstained with hematoxylin (blue). *A*, *B*, and *D–F*: signals from antisense probe. *C*: signals from antisense probe. BV, blood vessel; LP, lamina propria; N, nest; arrowheads, positive nucleated blood cells. *D*: image is a magnified area from the central, positive cells in *B*. *A*, *B*, and *D*: bar = 20 μm, magnification = ×40. *C*: bar = 20 μm, magnification = ×20. *E* and *F*: bar = 25 μm, magnification = ×40.

www.physiology.org/journal/ajprenal by ${individualUser.givenNames} ${individualUser.surname} (037.055.225.009) on June 10, 2018.
Copyright © 2010 American Physiological Society. All rights reserved.

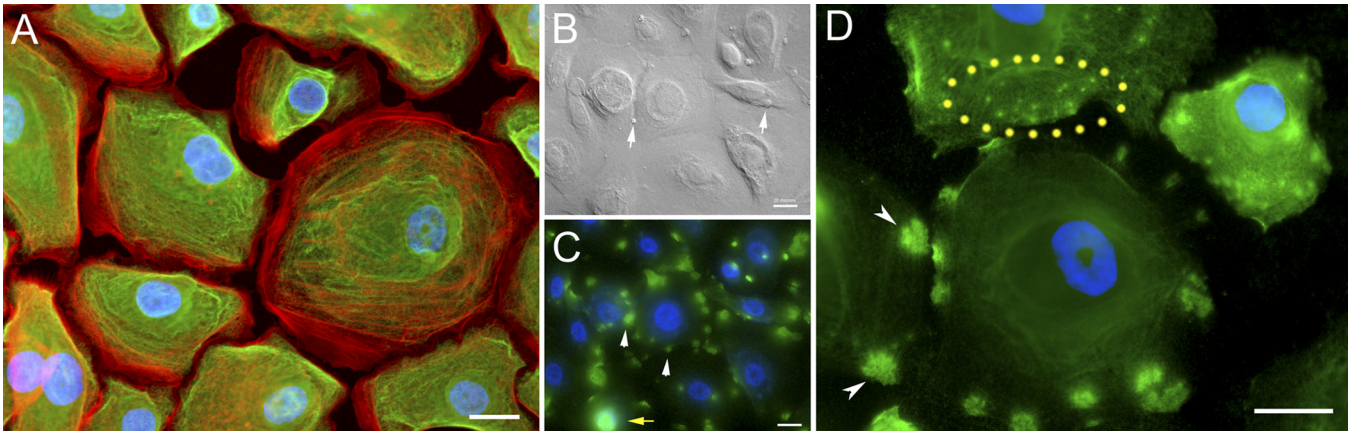

Fig. 12. Novel keratin immunostaining patterns are observed in epithelial cells cultured in vitro from the mucosa of the exstrophic bladder. Widefield fluorescence images are shown in *A*, *C*, and *D*. The differential interference contrast image shown in *B* corresponds to the widefield fluorescence image in *C*. Shown are immunoreactive profiles for K14 (green signal in *A*) and K7 (green signal in *C* and *D*). F-actin signals are displayed in red in *A*. DNA signals are displayed in blue in *A*, *C*, and *D*. *A*, *B*, and *C*: magnification = ×40. *D*: magnification = ×63. Yellow dotted ellipse in *D*, unique pattern of small K7-positive foci; yellow arrow in *C*, K7 dome; white arrowheads in *C* and *D*, unique pattern of ~5-μm K7-positive islands. Bar = 20 μm for all images.

intermediate filaments and hemidesmosomes, a property that could support detachment of basal urothelial cells from the urothelial basement membrane, migration into the lamina propria, and subsequent formation of von Brunn's nests. To address this hypothesis, colocalization analyses were performed on immunofluorescent signals derived from intermediate filaments and immunofluorescence signals derived from hemidesmosomes. Optical slices at the Rayleigh criterion were collected from the coverslip to 24 μm above the coverslip. The interface between cells and the extracellular matrix (ECM) was then examined for colocalization of keratin- and integrin-immunoreactive signals (Table 4) across multiple channels. We specifically calculated the Pearson's correlation coefficient, which ranges from −1 to 1 and indicates how well the signal intensities of the two channels being tested correlate to each other, In addition, Mander's overlap coefficient (range from 0 to 1), which shows the degree to which the signals of the two channels overlap, was calculated. For both coefficients, a score of 1 indicates perfect colocalization. Mean colocalization coefficients, generated from two colocalization experiments, are reported in Table 4. The exstrophic cell specimens were observed to exhibit nonsignificant coefficients, indicating a lack of colocalization between the selected keratins and hemidesmosomal proteins in this in vitro system. Normal urothelial cells, derived from the bladder mucosa of a vesicoureteral reflux patient, also failed to exhibit significant coefficients (Table 4). The collective data indicate that hemidesmosomes are not operational in this in vitro system and suggest that they are not disrupted in vivo.

DISCUSSION

von Brunn's nests, as well as its late developmental stages, cystitis cystica and cystitis glandularis, are proliferative and metaplastic disorders of the bladder mucosa rarely reported in children (7). The etiology of these disorders is not clear, but some observations state that their occurrence is often associated with chronic inflammation, irritation, and infection. Patients with bladder exstrophy (1), chronic indwelling urinary catheters (12, 52), pelvic lipomatosis (46), and chronic or recurrent urinary tract infection (8) are considered at risk. von Brunn's nests were not present in sections obtained from normal bladder biopsies, an observation shared by others (23, 24, 38). These observations were in contrast with results obtained by the study of Wiener et al. (55), which concluded that von Brunn's nests, cystitis, and nonkeratinizing squamous epithelium were found in great frequency in normal bladders. While 8/100 bladders were from subjects <21 yr of age, this study (55) failed to sufficiently survey pediatric bladders, thereby questioning its relevance to our report. In addition, the only

Table 3. *FGF-10 immunoreactivity in exstrophy specimens with von Brunn's nests, cystitis cystica, or squamous metaplasia*

Specimen	Urothelium	Von Brunn's Nest	Cystitis Cystica	Squamous Metaplasia
1	Focal, ±	NP	−	Focal, +++
2	NP	Focal, ±	NP	NP
3	Multifocal, +++	Multifocal, ±; diffuse, +++	NP	NP
4	NP	Diffuse, ±	NP	NP
5	Diffuse, +++	NP	Focal, ±	NP
6	NP	−	NP	NP
7	NP	Diffuse, ±	NP	NP

Tissue explants taken during the stage of the surgery listed. NP, not present. Immunoreactivity of FGF-10 in bladder exstrophy specimens that contain von Brunn's nests, cystitis cystica, or urothelium was given a subjective score by a pathologist (L. D. True) consisting of 2 dimensions: *1*) the pattern of signal in cells; and *2*) the strength of the signal (diffuse, focal, multifocal) and the intensity of signal in cells (−, negative, ± faint, or +++ intense).

www.physiology.org/journal/ajprenal by ${individualUser.givenNames} ${individualUser.surname} (037.055.225.009) on June 10, 2018.
Copyright © 2010 American Physiological Society. All rights reserved.

Table 4. *Analysis of colocalization between intermediate filament and hemidesmosomal proteins in exstrophic and normal bladder epithelial cells*

	Exstrophy *Specimen 1*				Exstrophy *Specimen 2*				Normal Bladder			
	IA6		L5		IA6		L5		IA6		L5	
	R_p	M	R_p	M	R_p	M	R_p	M	R_p	M	R_p	M
K7	0.01	0.02	0.04	0.06	0.12	0.15	0.13	0.05	0.01	0.03	0.08	0.09
K13	0.00	0.01	0.06	0.06	0.02	0.01	0.02	0.02	0.00	0.05	0.03	0.04
K14	0.02	0.03	0.08	0.09	0.00	0.00	0.05	0.06	0.01	0.02	0.10	0.11

Cells were grown on glass coverslips as described in MATERIALS AND METHODS. Shown is immunoreactivity with anti-integrin α6 (IA6) IgG, anti-laminin-5 (L5) IgG, and anti-keratin (K) IgG. R_p, Pearsons's correlation coefficient, scale −1 to 1; M, Manders overlap coefficient, scale 0 to 1. For both coefficients, score of 1 represents perfect colocalization.

condition for inclusion into the Weiner et al. study was "a normal appearance on gross inspection," a condition that obviously failed to appreciate pathological changes that could exclude specimens from the study.

In our study of pediatric bladders, Brunn's nests were prevalent only in bladder exstrophy patients. Exstrophy patients are at significantly increased risk to develop bladder cancer, and previous reports have implicated Brunn's nests as carcinoma precursors. Determining the origin and development of von Brunn's nests would address the role nests may play in carcinogenesis within the exstrophic bladder.

The origin of von Brunn's nest is not well understood, and the current literature is limited. Two models may be possible to explain the origin of the nests: *1*) direct invasion of normal urothelial cells and *2*) formation from other cell types. In support of the first model, Goldstein et al. (18) observed that under the influence of a strong repair stimulus, connective tissue underlying the urothelium became loose and urothelial cells underwent numerous mitoses. This raises the possibility that isolated cells from the urothelium can drop off into the lamina propria where they multiply and form nests of cells. Noda and Eto (36) tried to reveal the mechanisms for nest formation and stated that chronic stimulation with inflammation or physical stimulation with crystals or calculi caused the urothelium to form nests. These nests were isolated as the result of an adhesive occlusion of the urothelium at the orifice of the nest (36). Serial sectioning through the entire mucosa has allowed some investigators to predict that von Brunn's nests are epithelial growths extending down from the urothelium (9). Our biopsied specimens, however, do not exhibit this phenomenon because we studied sufficient adjacent sections to conclude that we are not simply looking at the ends of a downgrowth. Some nested islands reported in our study are in close proximity to the epithelium, but none of the nests exhibit obvious continuity with bladder urothelium. With respect to the second model, 10pRp cells that form clusters in the lamina propria would not be expected to generate structures that would find a way to attach to the urothelium.

Our immunostaining results showed that von Brunn's nest, like normal urothelium, is K17 positive, suggesting that nested cells share some of the same intermediate filament properties as transitional epithelium. These results seem to support the first model. Some of our in situ hybridization data also support this model. The probe used for the in situ hybridization was synthesized from exon 8 of the *FGFR2* gene to specifically detect the IIIb mRNA splice variant encoding the FGF-10 receptor (isoform 2 in the NCBI nomenclature). In normal bladder tissue, only urothelial cells and smooth muscle cells exhibit positive signals for the receptor mRNA (58). Since smooth muscle bundles are easily identified from other cell types, the IIIb mRNA splice variant and its translated type 2 isoform can now be considered as a marker for urothelial cells. In this study, we found that the nested cells express the FGF-10 receptor, just like urothelial cells of normal and exstrophic transitional epithelium. We also found that some cells in close proximity to von Brunn's nests also exhibited positive signals for the receptor at both protein and mRNA levels. This would seem to indicate that the nests are derivatives of urothelial cells that have proliferated in the lamina propria. This supposition, however, ignores the 10pRp cells we identified and the distribution of the receptor-positive cells. Our K7 immunostaining data also contradict this. K7 is an epithelial marker whose expression occurs even at the very early stages of bladder urothelium differentiation (54). Our data indicate that a subset of young nests are K7 negative. This result implies the nested cells are not directly derived from the normal urothelium and questions the "pinching off" model in our exstrophic specimens.

Hemidesmosomes attach the intermediate filaments of basal cells to the underlying extracellular matrix (ECM), essentially anchoring the cells to the basement membrane. If the hemidesmosomes within the urothelium were not properly functioning, basal cells could disconnect from the ECM, leaving open the possibility that they might cross the basement membrane and escape into the lamina propria. From here, these individual cells could develop into von Brunn's nests, suggesting that FGF-10 receptor-positive cells observed within the lamina propria were urothelial in nature. Our data do not support involvement of hemidesmosomes in the pathobiology of von Brunn's nest formation and, accordingly, do not support the first model.

Our in situ hybridization results show that within the normal area of the lamina propria, cells positive for the mRNA encoding the FGF-10 receptor are not detectable. Within areas proximal to von Brunn's nests, however, this profile changes. There are individual cells, clustered cells, and nested cells that are positive for the FGFR2IIIb mRNA splice variant. The clustered cells represent a possible starting point of nest development, with 10pRp cells and fibroblasts serving as a probable initial source of cells for the clusters. If the second model represents the mechanism of nest formation, a primary picture here seems that the 10pRp cells were transported through blood vessels to the site of

RIGHTSLINK www.physiology.org/journal/ajprenal by ${individualUser.givenNames} ${individualUser.surname} (037.055.225.009) on June 10, 2018.
Copyright © 2010 American Physiological Society. All rights reserved.

nest formation to respond to inflammation. They then form the cluster and subsequent nest to seal or isolate the site. This may be the original protective function of the nests. It is noted that our evidence does not directly implicate the bloodstream as a vehicle for 10pRp cells to travel through.

During nest maturation, cells of the von Brunn's nests may be exposed to stimulation by inflammatory factors. This scenario is supported by changes in K7 immunostaining patterns that accompany the change from a group of nested cells to a urothelial-like morphology that accompanies the formation of a lumen within the nest. Another possibility which cannot be excluded is the combination of the two models. If small amounts of urothelial cells can make their way into the lamina propria by "dropping off" (as opposed to "pinching off"), the functions of stem cells and their derivatives, such as lymphocytes and monocytes, may promote nest formation and further development by infiltrating into nested cells, increasing cell numbers, and adopting a urothelial-like morphology and structure. It is of interest that we note the ability of "spore-like stem cells," also referred to as very small embyronic-like stem cells (VSELs), which possess the ability to replicate and differentiate into the cell type present in the tissue (41, 50, 51, 59, 60). Once the nests form, their growth relies on the proliferation of the nested cells. Although the relationship between 10pRp cells and stem cells remains to be determined, the possibility that 10pRp cells might provide inductive activity to VSELs is intriguing. Even more intriguing is the possibility that 10pRp cells develop directly from spore-like or VSEL stem cells.

We have previously shown that FGF-10 expressed in lamina propria is a paracrine mitogen for urothelial cell growth (2, 58). In this study, we detected strong FGF-10 signals in the nests and revealed that the nested cells also possess the ability to synthesize the mRNA and protein of the FGF-10 receptor. This signal transduction pathway seems to be the basis of the nest growth and further development into its later stages, cystitis cystica and cystitis glandularis. Based on immunoreactive signals, FGF-10 was found to be abundant in some, but not all, nuclei of cells of the von Brunn's nest and urothelial cells of transitional epithelium. The collective evidence points to a mechanism where the 10pRp cells develop into von Brunn's nests under the control of the FGF-10 signal transduction system. Convincing proof that 10pRp cells can develop into von Brunn's nests will require such experiments as injecting genetically defined 10pRp cells (perhaps as xenografts) and the subsequent demonstration that these cells populate von Brunn's nests.

The literature is devoid of reports that indicate that infants undergoing an anatomic reconstruction of an exstrophic bladder in the first few weeks or months of life are at increased risk of developing bladder cancer later in life. Data do exist to support an increased risk of bladder cancer for patients with *1*) unreconstructed bladder exstrophy, *2*) delayed repair of bladder exstrophy, or *3*) reconstruction with bowel or a ureterosigmoidostomy. Also, the data surrounding patients after augmentation cystoplasty and their risk for cancer are becoming less clear as we recognize that patients on any catheterization regimen of the bladder may be at increased risk of bladder cancer with or without enterocystoplasty.

Nearly one-half of bladder carcinomas are derived from benign lesions where environmental, social, hereditary, and cell biological changes come together to initiate and promote irreversible changes. Reactive changes in the epithelium of von Brunn's nests are therefore capable of leading to serious and deleterious consequences. Such changes to the epithelium that lead to von Brunn's nests include chronic inflammation, congenital anomalies, infection with *Schistosoma hematobium* (33), and the repeated surgical closure of exstrophic bladders (37). It is significant that our study describes von Brunn's nests before any surgical intervention to correct the exstrophic birth defect. The exstrophic condition thus appears to have hijacked the FGF-10 signal transduction system to serve as the principal mitogenic mechanism which underlies the proliferation and development of von Brunn's nests in the exstrophic bladder.

ACKNOWLEDGMENTS

The authors acknowledge Eric Rubio, Kimberly Cochrane, Shelly Bagai, and Nicole Carmean Jacobs for excellent technical assistance. We are grateful to Dr. Elaine Fuchs (Rockefeller University) for providing a breeding pair of FGF-7 (−/−) mice. The generosity of Drs. Jeff Rubin (National Institutes of Health) and Andrew Farr (University of Washington) in providing newborn specimens of FGF10-null mice is acknowledged. The authors acknowledge Dr. Jonathan Jones for the kind gift of antiserum to laminin-5. J. A. Bassuk is especially appreciative of Dr. Jennifer Southgate and Jennifer Henley Butcher (University of York, Heslington, UK) for expert instruction in immunohistochemical applications and keratin profiling in the study of epithelial differentiation.

Present addresses: E. M. Leaf, Dept. of Bioengineering, Univ. of Washington, Seattle, WA; R. M. Sweet, Dept. of Urologic Surgery, Univ. of Minnesota, Minneapolis, MN; M. E. Mitchell, Dept. of Urology, Medical College of Wisconsin, WI.

GRANTS

The study was supported by National Institute of Diabetes and Digestive and Kidney Diseases Grants R01DK062251, R01DK08881, and UO1DK065202 (ancillary project) to J. A. Bassuk.

DISCLOSURES

No conflicts of interest, financial or otherwise, are declared by the authors.

REFERENCES

1. **Al Ahmadie H, Gomez AM, Trane N, Bove KE.** Giant botryoid fibroepithelial polyp of bladder with myofibroblastic stroma and cystitis cystica et glandularis. *Pediatr Dev Pathol* 6: 179–181, 2003.
2. **Bagai S, Rubio E, Cheng JF, Sweet R, Thomas R, Fuchs E, Grady R, Mitchell M, Bassuk JA.** Fibroblast growth factor-10 is a mitogen for urothelial cells. *J Biol Chem* 277: 23828–23837, 2002.
3. **Bassuk JA, Birkebak T, Rothmier JD, Clark JM, Bradshaw A, Muchowski PJ, Howe CC, Clark JI, Sage EH.** Disruption of the *Sparc* locus in mice alters the differentiation of lenticular epithelial cells and leads to cataract formation. *Exp Eye Res* 68: 321–331, 1999.
4. **Bassuk JA, Grady R, Mitchell M.** The molecular era of bladder research. Transgenic mice as experimental tools in the study of outlet obstruction. *J Urol* 164: 170–179, 2000.
5. **Beare JB, Tormey AR Jr, Wattenberg CA.** Exstrophy of the urinary bladder complicated by adenocarcinoma. *J Urol* 76: 583–594, 1956.
6. **Bryan RT, Nicholls JH, Harrison RF, Jankowski JA, Wallace DM.** The role of beta-catenin signaling in the malignant potential of cystitis glandularis. *J Urol* 170: 1892–1896, 2003.
7. **Capozza N, Collura G, Nappo S, de Dominicis M, Francalanci P, Caione P.** Cystitis glandularis in children. *BJU Int* 95: 411–413, 2005.
8. **Chen Z, Ye Z, Zeng W.** Clinical investigation on the correlation between lower urinary tract infection and cystitis glandularis. *J Huazhong Univ Sci Technolog Med Sci* 24: 303–304, 2004.
9. **Cohen SM.** Comparative pathology of proliferative lesions of the urinary bladder. *Toxicol Pathol* 30: 663–671, 2002.
10. **Corica FA, Husmann DA, Churchill BM, Young RH, Pacelli A, Lopez-Beltran A, Bostwick DG.** Intestinal metaplasia is not a strong risk

RIGHTSLINK www.physiology.org/journal/ajprenal by ${individualUser.givenNames} ${individualUser.surname} (037.055.225.009) on June 10, 2018.
Copyright © 2010 American Physiological Society. All rights reserved.

factor for bladder cancer: study of 53 cases with long-term follow-up. *Urology* 50: 427–431, 1997.
11. **Davies G, Castro JE.** Cystitis glandularis. *Urology* 10: 128–129, 1977.
12. **Delnay KM, Stonehill WH, Goldman H, Jukkola AF, Dmochowski RR.** Bladder histological changes associated with chronic indwelling urinary catheter. *J Urol* 161: 1106–1108, 1999.
13. **Deng FM, Liang FX, Tu L, Resing KA, Hu P, Supino M, Hu CC, Zhou G, Ding M, Kreibich G, Sun TT.** Uroplakin IIIb, a urothelial differentiation marker, dimerizes with uroplakin Ib as an early step of urothelial plaque assembly. *J Cell Biol* 159: 685–694, 2002.
14. **Dinney CP, Ramirez EI, Swanson DA, Ro JY, Babaian RJ, von Eschenbach AC.** Management of transitional cell carcinoma involving von Brunn's nests. *J Urol* 153: 944–949, 1995.
15. **Edwards PD, Hurm RA, Jaeschke WH.** Conversion of cystitis glandularis to adenocarcinoma. *J Urol* 108: 568–570, 1972.
16. **Fairbanks TJ, De Langhe S, Sala FG, Warburton D, Anderson KD, Bellusci S, Burns RC.** Fibroblast growth factor 10 (Fgf10) invalidation results in anorectal malformation in mice. *J Pediatr Surg* 39: 360–365, 2004.
17. **Garthwaite MA, Thomas DF, Subramaniam R, Stahlschmidt J, Eardley I, Southgate J.** Urothelial differentiation in vesicoureteric reflux and other urological disorders of childhood: a comparative study. *Eur Urol* 49: 154–160, 2006.
18. **Goldstein AM, Fauer RB, Chinn M, Kaempf MJ.** New concepts on formation of Brunn's nests and cysts in urinary tract mucosa. *Urology* 11: 513–517, 1978.
19. **Guo L, Degenstein L, Fuchs E.** Keratinocyte growth factor is required for hair development but not for wound healing. *Genes Dev* 10: 165–175, 1996.
20. **Guo L, Yu QC, Fuchs E.** Targeting expression of keratinocyte growth factor to keratinocytes elicits striking changes in epithelial differentiation in transgenic mice. *EMBO J* 12: 973–986, 1993.
21. **Harnden P, Southgate J.** Cytokeratin 14 as a marker of squamous differentiation in transitional cell carcinomas. *J Clin Pathol* 50: 1032–1033, 1997.
22. **Jones JC.** Hemidesmosomes in bladder epithelial cells. *Urology* 57: 103, 2001.
23. **Jost SP, Gosling JA, Dixon JS.** The fine structure of Brunn's nests in human bladder urothelium. *J Submicrosc Cytol Pathol* 22: 203–210, 1990.
24. **Knowles MA, Hicks RM, Berry RJ, Milroy E.** Organ culture of normal human bladder: choice of starting material and culture characteristics. In: *Methods in Cell Biology*. London, UK: Academic, 1980.
25. **Kosman J, Carmean N, Leaf EM, Dyamenahalli K, Bassuk JA.** Translocation of fibroblast growth factor-10 and its receptor into nuclei of human urothelial cells. *J Cell Biochem* 102: 769–785, 2007.
26. **Kruger V, Khoshvaghti M, Reutter H, Vogt H, Boemers TM, Ludwig M.** Investigation of FGF10 as a candidate gene in patients with anorectal malformations and exstrophy of the cloaca. *Pediatr Surg Int* 24: 893–897, 2008.
27. **Lendvay TS, Sweet R, Han CH, Soygur T, Cheng JF, Plaire JC, Charleston JS, Charleston LB, Bagai S, Cochrane K, Rubio E, Bassuk JA.** Compensatory paracrine mechanisms that define the urothelial response to injury in partial bladder outlet obstruction. *Am J Physiol Renal Physiol* 293: F1147–F1156, 2007.
28. **Medina PM, Valero Puerta JA, Valpuesta F, I, Sanchez GM.** Bladder adenocarcinoma with glandular cystitis areas. *Arch Esp Urol* 54: 254–256, 2001.
29. **Min H, Danilenko DM, Scully SA, Bolon B, Ring BD, Tarpley JE, DeRose M, Simonet WS.** Fgf-10 is required for both limb and lung development and exhibits striking functional similarity to *Drosophila* branchless. *Genes Dev* 12: 3156–3161, 1998.
30. **Moll R, Achtstatter T, Becht E, Balcarova-Stander J, Ittensohn M, Franke WW.** Cytokeratins in normal and malignant transitional epithelium. Maintenance of expression of urothelial differentiation features in transitional cell carcinomas and bladder carcinoma cell culture lines. *Am J Pathol* 132: 123–144, 1988.
31. **Moll R, Divo M, Langbein L.** The human keratins: biology and pathology. *Histochem Cell Biol* 129: 705–733, 2008.
32. **Moll R, Franke WW, Schiller DL, Geiger B, Krepler R.** The catalog of human cytokeratins: patterns of expression in normal epithelia, tumors and cultured cells. *Cell* 31: 11–24, 1982.
33. **Mostafa MH, Sheweita SA, O'Connor PJ.** Relationship between schistosomiasis and bladder cancer. *Clin Microbiol Rev* 12: 97–111, 1999.
34. **Mostofi FK.** Potentialities of bladder epithelium. *J Urol* 71: 705–714, 1954.
35. **Murphy DP, Pantuck AJ, Amenta PS, Das KM, Cummings KB, Keeney GL, Weiss RE.** Female urethral adenocarcinoma: immunohistochemical evidence of more than 1 tissue of origin. *J Urol* 161: 1881–1884, 1999.
36. **Noda S, Eto K.** Histopathological studies on the cystic formation of the human urothelium. *Kurume Med J* 37: 55–65, 1990.
37. **Novak TE, Lakshmanan Y, Frimberger D, Epstein JI, Gearhart JP.** Polyps in the exstrophic bladder. A cause for concern? *J Urol* 174: 1522–1526, 2005.
38. **Schade RO, Swinney J.** Pre-cancerous changes in bladder epithelium. *Lancet* 2: 943–946, 1968.
39. **Schweizer J, Bowden PE, Coulombe PA, Langbein L, Lane EB, Magin TM, Maltais L, Omary MB, Parry DA, Rogers MA, Wright MW.** New consensus nomenclature for mammalian keratins. *J Cell Biol* 174: 169–174, 2006.
40. **Shirai T, Fukushima S, Hirose M, Ohshima M, Ito N.** Epithelial lesions of the urinary bladder in three hundred and thirteen autopsy cases. *Jpn J Cancer Res* 78: 1073–1080, 1987.
41. **Shmilovici A.** Mammalian spore-like cells—a reservoir of spare parts for old-age? *Med Hypotheses* 68: 767–769, 2007.
42. **Singh I, Ansari MS.** Cystitis cystica glandularis masquerading as a bladder tumor. *Int Urol Nephrol* 33: 635–636, 2001.
43. **Smeulders N, Woodhouse CR.** Neoplasia in adult exstrophy patients. *BJU Int* 87: 623–628, 2001.
44. **Southgate J, Harnden P, Selby PJ, Thomas DFM, Trejdosiewicz LK.** Urothelial Tissue Regulation: Unraveling the Role of the Stroma. In: *Advances in Bladder Research*, edited by Baskin LS and Hayward SW. New York: Kluwer Academic/Plenum, 1999.
45. **Southgate J, Harnden P, Trejdosiewicz LK.** Cytokeratin expression patterns in normal and malignant urothelium: a review of the biological and diagnostic implications. *Histol Histopathol* 14: 657–664, 1999.
46. **Sozen S, Gurocak S, Uzum N, Biri H, Memis L, Bozkirli I.** The importance of re-evaluation in patients with cystitis glandularis associated with pelvic lipomatosis: a case report. *Urol Oncol* 22: 428–430, 2004.
47. **Spinardi L, Marchisio PC.** Podosomes as smart regulators of cellular adhesion. *Eur J Cell Biol* 85: 191–194, 2006.
48. **Spinardi L, Rietdorf J, Nitsch L, Bono M, Tacchetti C, Way M, Marchisio PC.** A dynamic podosome-like structure of epithelial cells. *Exp Cell Res* 295: 360–374, 2004.
49. **Tash JA, David SG, Vaughan EDE, Herzlinger DA.** Fibroblast growth factor-7 regulates stratification of the bladder urothelium. *J Urol* 166: 2536–2541, 2001.
50. **Vacanti MP, Roy A, Cortiella J, Bonassar L, Vacanti CA.** Identification and initial characterization of spore-like cells in adult mammals. *J Cell Biochem* 80: 455–460, 2001.
51. **Vacanti MP, Vacanti CA.** Spore-like cells and uses thereof. *US* Patent #7575921, issued August 18, 2009.
52. **Vaidyanathan S, Mansour P, Soni BM, Singh G, Sett P.** The method of bladder drainage in spinal cord injury patients may influence the histological changes in the mucosa of neuropathic bladder—a hypothesis. *BMC Urol* 2: 5, 2002.
53. **Varley CL, Stahlschmidt J, Smith B, Stower M, Southgate J.** Activation of peroxisome proliferator-activated receptor-gamma reverses squamous metaplasia and induces transitional differentiation in normal human urothelial cells. *Am J Pathol* 164: 1789–1798, 2004.
54. **Veranic P, Romih R, Jezernik K.** What determines differentiation of urothelial umbrella cells? *Eur J Cell Biol* 83: 27–34, 2004.
55. **Wiener DP, Koss LG, Sablay B, Freed SZ.** The prevalence and significance of Brunn's nests, cystitis cystica and squamous metaplasia in normal bladders. *J Urol* 122: 317–321, 1979.
56. **Woodhouse CR, North AC, Gearhart JP.** Standing the test of time: long-term outcome of reconstruction of the exstrophy bladder. *World J Urol* 24: 244–249, 2006.
57. **Yucel S, Liu W, Cordero D, Donjacour A, Cunha G, Baskin LS.** Anatomical studies of the fibroblast growth factor-10 mutant, Sonic Hedge Hog mutant and androgen receptor mutant mouse genital tubercle. *Adv Exp Med Biol* 545: 123–148, 2004.
58. **Zhang D, Kosman J, Carmean N, Grady R, Bassuk JA.** FGF-10 and its receptor exhibit bidirectional paracrine targeting to urothelial and smooth muscle cells in the lower urinary tract. *Am J Physiol Renal Physiol* 291: F481–F494, 2006.
59. **Zuba-Surma EK, Kucia M, Ratajczak J, Ratajczak MZ.** "Small stem cells" in adult tissues: very small embryonic-like stem cells stand up! *Cytometry A* 75: 4–13, 2009.
60. **Zuba-Surma EK, Ratajczak MZ.** Overview of very small embryonic-like stem cells (VSELs) and methodology of their identification and isolation by flow cytometric methods. *Curr Protoc Cytom Chapter* 9: Unit 9, 2010.

RIGHTSLINK www.physiology.org/journal/ajprenal by ${individualUser.givenNames} ${individualUser.surname} (037.055.225.009) on June 10, 2018.
Copyright © 2010 American Physiological Society. All rights reserved.